AD-A152 382 THE DEVELOPMENT OF LASER ANALYTICAL METHODS FOR THE CHARACTERIZATION OF S..(U) NORTHWESTERN UNIV EVANSTON IL Y W CHUNG ET AL. FEB 85 N00014-79-C-0794 1/1

UNCLASSIFIED F/G 7/4 NL

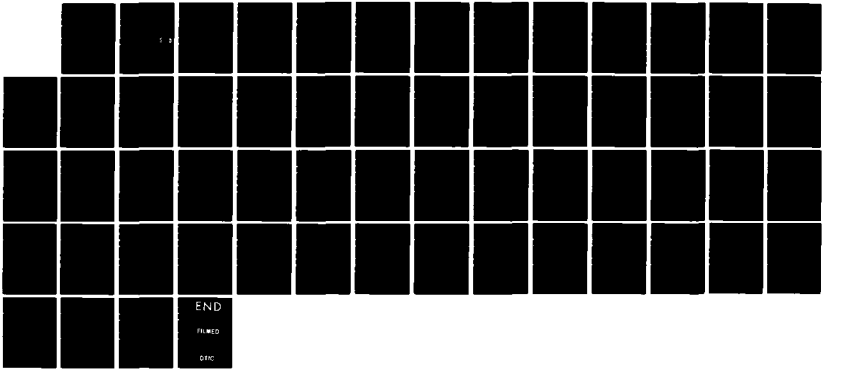

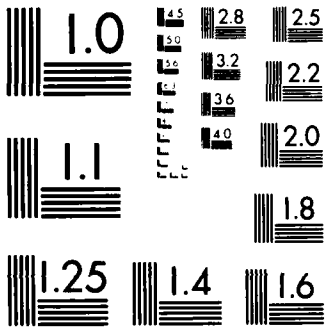

SECURITY CLASSIFICATION OF THIS PAGE (When Data Entered)

REPORT DOCUMENTATION PAGE

READ INSTRUCTIONS BEFORE COMPLETING FORM

1. REPORT NUMBER	2. GOVT ACCESSION NO.	3. RECIPIENT'S CATALOG NUMBER

4. TITLE (and Subtitle)
The Development of Laser Analytical Methods for the Characterization of Solid/Liquid and Solid/High Pressure Gas Interfaces

5. TYPE OF REPORT & PERIOD COVERED
Final - Sept. 1, 1979 to June 30, 1983

6. PERFORMING ORG. REPORT NUMBER

7. AUTHOR(s)
Y.W. Chung, G.C. Schatz, P.C. Stair, R.P. Van Duyne, E. Weitz

8. CONTRACT OR GRANT NUMBER(s)
N00014-79-C-0794

9. PERFORMING ORGANIZATION NAME AND ADDRESS
Departments of Chemistry and Materials Science and Engineering
Northwestern University, Evanston, IL 60201

10. PROGRAM ELEMENT, PROJECT, TASK AREA & WORK UNIT NUMBERS

11. CONTROLLING OFFICE NAME AND ADDRESS
Office of Naval Research
Department of the Navy
Arlington, VA 22217

12. REPORT DATE
February, 1985

13. NUMBER OF PAGES

14. MONITORING AGENCY NAME & ADDRESS(if different from Controlling Office)

15. SECURITY CLASS. (of this report)
Unclassified

15a. DECLASSIFICATION/DOWNGRADING SCHEDULE

16. DISTRIBUTION STATEMENT (of this Report)
Approved for public release; distribution unlimited

17. DISTRIBUTION STATEMENT (of the abstract entered in Block 20, if different from Report)

18. SUPPLEMENTARY NOTES

19. KEY WORDS (Continue on reverse side if necessary and identify by block number)
pulsed laser thermal induced desorption,
carbon monoxide
Cu(100)
surface diffusion
surface enhanced Raman spectroscopy,
surface enhanced Resonance Raman spectroscopy,
fluorescence quenching,
electromagnetic theory,
time dependent Hartree Fock.

20. ABSTRACT (Continue on reverse side if necessary and identify by block number)
This report summarizes research in two areas: laser induced thermal desorption at solid/UHV interfaces, and surface enhanced optical spectroscopy at solid/liquid, solid/gas and solid/UHV interfaces. The major accomplishment in the first area was the development of a pulsed laser induced thermal desorption technique for probing surface desorption and diffusion. In the second area, an apparatus has been constructed which enables the measurement of surface enhanced Raman and other surface optical spectra in UHV. In addition, surface enhanced
(cont'd on other side)

DD FORM 1 JAN 73 1473 EDITION OF 1 NOV 65 IS OBSOLETE
S/N 0102-014-6601

SECURITY CLASSIFICATION OF THIS PAGE (When Data Entered)

20. (cont'd from other side)

spectra were measured for a number of adsorbate/substrate combinations in electrochemical cells, and the theory of surface enhancement effects was elucidated.

FINAL REPORT

The Development of Laser Analytical Methods for the Characterization of Solid/Liquid and Solid/High Pressure Gas Interfaces

Y.W. Chung, G.C. Schatz, P.C. Stair
R.P. Van Duyne and E. Weitz

Departments of Chemistry and Materials
Science and Engineering, Northwestern University,
Evanston, IL 60201

Prepared for

Office of Naval Research
Department of the Navy

under

Contract N00014-79-C-0794

February, 1985

Table of Contents

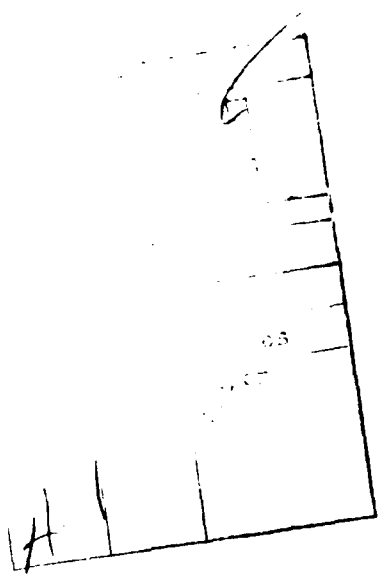

I. Introduction

This final report summarizes the accomplishments associated with scientific research supported by ONR Contract N00014-79-C-0794. This contract commenced on September 1, 1979 and ended on June 30, 1983. It was funded out of ONR's Selected Research Opportunities (SRO) Program. The research involved a collaboration between five faculty (Y.W. Chung, P.C. Stair, G.C. Schatz, R.P. Van Duyne and E. Weitz) who are from the Departments of Chemistry and Materials Science and Engineering at Northwestern University.

The overall goal of the research was to develop laser-based methods for characterizing molecules at interfaces. Two general classes of methods were considered: (1) pulsed laser induced thermal desorption, and (2) surface enhanced optical spectroscopy. Among the important accomplishments of this research was the development of instrumentation which enables measurements at solid/UHV interfaces using both methods. Primary applications of the laser induced desorption technique were to measurements of surface diffusion coefficients for molecules adsorbed on copper surfaces, and to the analysis of time of flight spectra of the desorbed molecules. Applications of surface enhanced optical spectroscopy included surface enhanced Raman and resonance Raman studies of molecules adsorbed on Group IB metals in UHV, air and electrochemical systems. Surface induced fluorescence quenching, and surface enhanced second, third and fourth harmonic generation were also studied. Associated with several aspects of the experimental work were theoretical studies designed to guide and interpret the experiments. A major result of the theoretical work was the elucidation of the mechanisms responsible for surface enhancement effects in spectroscopic studies of Group IB metals.

A more detailed summary of the research accomplishments under N00014-79-C-0794 is given in the next two sections. Section V lists the 23 publications that have resulted from this research while Section VI lists the students, post-doctorals and others who worked under this contract.

It is probably accurate to conclude that the methods, ideas and results that emanated from this contract would probably never have been possible without the extensive collaboration between scientists in several different disciplines that this project made possible.

II. Pulsed Laser-Induced Thermal Desorption

A major objective of the work supported by ONR was development of a pulsed laser-induced thermal desorption technique (PLID) to probe the dynamics of surface processes [1], [2], [3], [4]. An understanding of pulsed laser-induced thermal desorption is best obtained with reference to ordinary thermal desorption spectroscopy. In ordinary thermal desorption the surface temperature is raised according to some specified time program until all adsorbed molecules have desorbed. In PLID, a pulsed laser is incident on a surface which absorbs all or part of the energy in the laser pulse. The absorbed energy is rapidly converted into heat which raises the surface temperature. The surface temperature returns to ambient following the laser pulse at a rate which depends principally upon the amount of energy deposited and the thermal conductivity of the material. The maximum temperature reached by the surface also depends upon the thermal conductivity, the laser flux, pulse length, and surface absorption coefficient at the laser frequency. The elevated temperature produced by the laser pulse can induce desorption of molecules adsorbed on the surface. However, some threshold temperature must be achieved before any desorption occurs. As the laser flux is increased beyond the value necessary to reach this threshold, a progressively larger fraction of the adsorbed molecules in the irradiated area are desorbed. This leads to an increasing amplitude of the desorption signal as measured by a mass analyzer detector or other pressure sensor. Eventually, for sufficiently high power densities, the desorption signal levels off when all of the adsorbed molecules in the irradiated area are removed by the pulse. The main differences between PLID and ordinary thermal desorption are: (1) PLID heating rates are much higher, typically 10^8 - 10^{11} degrees per second and, (2) only a fraction of the surface need be heated by the laser pulse since thermal diffusion lengths are short on the time scale of the heating.

In the work supported by ONR we have utilized the pulsed, localized heating characteristics of PLID to investigate the dynamics of carbon monoxide desorption from clean copper surfaces and to observe the diffusion of CO across the copper surface. In the former case, we have taken advantage of fast heating and cooling to create a pulse of desorbed molecules at a well-defined time. By measuring the time-of-flight (TOF) into a mass spectrometer following the heat pulse, we have determined the translational energy distribution and hence the energy transferred into this molecular degree of freedom. In the latter case we have also utilized the spatial resolution of the heating to create a concentration hole in the adsorbate layer. The filling in of this hole with time is monitored by subsequent pulsed desorption giving a direct observation of surface diffusion.

Experiments were carried out in a two chamber UHV apparatus (see Fig. 1) which has been described in detail in reference [4]. The main ion pumped

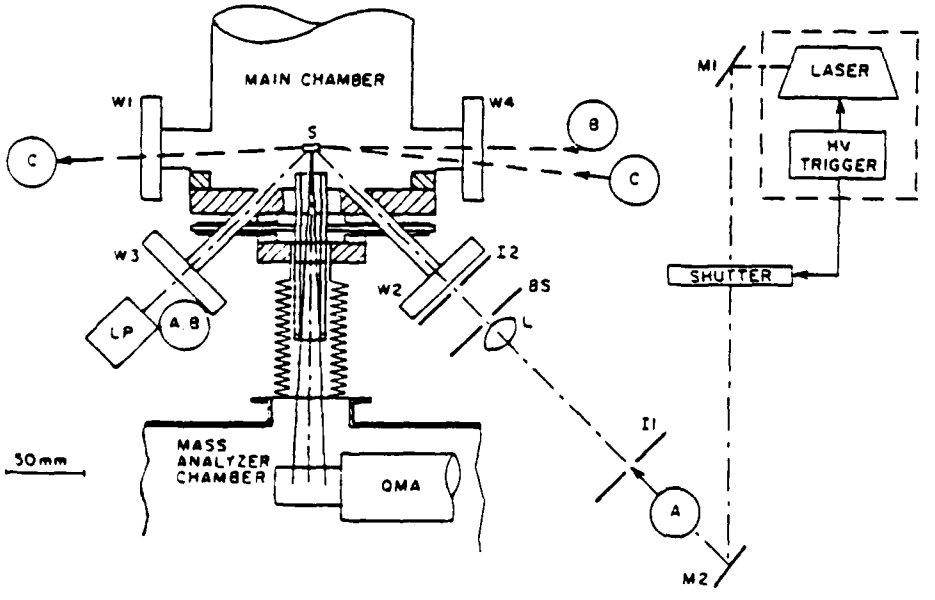

FIG. 1 The parts of the apparatus directly relevant to a time-of-flight experiment are shown. The laser beam is reflected off mirror M1 to a shutter which selects out pulses at appropriate time intervals which are then directed to the surface via irises I_1 and I_2. The beam splitter picks off a portion of the incident beam for power monitoring. The beam path shown (A) involves windows W2 and W3 but could also involve W4 + W3 (B) or W4 + W1 (C). The energy of the beam is measured by a laser power meter (LP) after exiting the chamber.

chamber contained the Cu sample mounted via wires on a manipulator with facilities for electron beam heating and liquid nitrogen cooling the sample. The temperature of the sample as measured by a Chromel-Alumel thermocouple could be varied between 80 and 1000 K. An ion sputter gun, ion gauge, and differentially pumped BaF_2 windows are also mounted on the chamber. The second turbomolecular pumped chamber contained a quadrupole mass analyzer with the ionizer situated in line of site to the sample surface. The second chamber was connected to the first by a flexible bellows which permitted the flight distance to be adjusted. To minimize detection of molecules which do not follow a direct line-of-sight path from surface to detector, liquid nitrogen cooled irises were placed between the sample and the ionizer for TOF measurements. An excimer laser at the KrF wavelength (248 nm) with a pulse width of 1.5×10^{-8} seconds and single pulse energies of 0-5mJ was used for most of the experiments. The laser beam was focused to a spot 0.1 - 1 mm diameter on the copper surface in order to flash heat the sample and desorb CO. Real time distributions of the desorbed CO arriving at the mass spectrometer were obtained with a transient recorder - signal averager combination. The quantity of desorbed CO was determined from the amplitude of the measured desorption pulse.

TOF spectra have been measured as a function of CO coverage, laser power density, and initial surface temperature. In order to analyze the data with minimal prejudice, the observed velocity distributions were least-squares fit to a modified Maxwell-Boltzmann expression:

$$N(v) = v^4 \exp[-(a + bv + cv^2)]$$

where a is a normalization constant and b characterizes the deviation from a Boltzmann velocity distribution. T the temperature can be defined as $T = \langle E \rangle / 2K$. This function reduces to a Maxwell-Boltzmann distribution for b=0 and c=M/2kT. From the fitted velocity distribution, the quantity $\langle E^2 \rangle / \langle E \rangle^2 = 1 +$

$w^2/2$ can be defined. w is similar to the reduced speed ratio of the distribution and physically represents the width of the energy distribution. A Maxwell-Boltzmann distribution has w=1. For our typical distributions w = 1.00 to within 0.05. Thus our TOF distributions are well fit by a Maxwell-Boltzmann distribution, and the resulting temperature can be discussed as a true translational temperature. Fig. 2 shows the observed signals and fits for two representative desorption fluxes. We obtain similar fits to a Boltzmann distribution

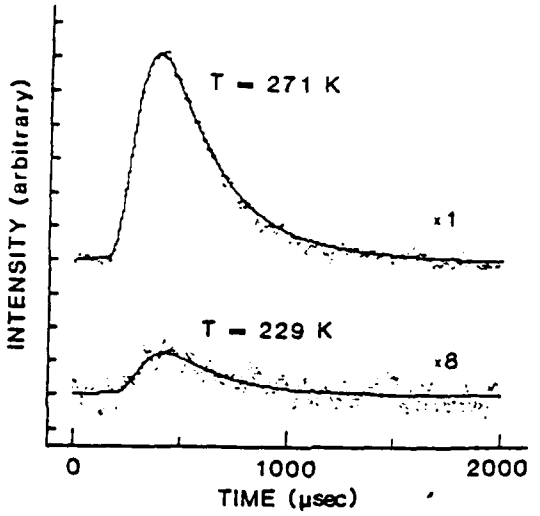

FIG. 2. Time-of-flight distribution for CO desorbing from Cu(100). The initial surface temperature was 90 K and the time-of-flight distance was 218 nm. The upper curve corresponds to saturation coverage of CO. The laser power density of 44 MW/cm^2 resulted in desorption of all of the adsorbates within the laser irradiated region. The fitted TOF temperature is 271 ± 1 K and $W = 1.06 \pm 0.01$ where the error limits are the standard deviations on the fit. For the power curve the coverage was 0.25 saturation. The laser power density of 9 MW/cm^2 resulted in desorption of 10% of the adsorbates within the laser irradiated area. The fitted TOF temperature is 229 ± 7 K and $W = 0.97 \pm 0.06$. The lower curve has been expanded eightfold relative to the top curve and thus corresponds to 0.025 of the desorbed flux of the top curve.

for all coverages and for all incident power levels from the threshold for desorption to laser powers where all adsorbed molecules within the irradiation area are desorbed in a single pulse.

The surface temperature at the point of CO desorption cannot be measured, but a good estimate of the surface temperature is obtained from the kinetic parameters for CO desorption measured by ordinary thermal desorption. We have performed ordinary thermal desorption measurements for the CO/Cu(100) system. We find a coverage dependent activation energy (65 - 40 kJ/mol) nearly equal to the coverage dependent heat of adsorption reported previously [5]. The pre-exponential factor is coverage independent to within the accuracy of our data. The surface temperature for CO desorption calculated using these kinetic parameters and a heat pulse appropriate for pulsed laser heating is in the range 400 - 600 K with the peak desorption rate at 510 K. Therefore, our measured translational temperatures are significantly lower than the surface temperature at point of desorption.

One possible explanation for the difference between the measured translational temperatures and the calculated surface temperatures could be that the TOF data does not represent the nascent distribution of velocities for desorbing CO. Indeed, for high CO desorption fluxes the molecules experience collisions in the gas phase above the surface because of the high densities produced by short desorption times. However, a calculation of the effect of collisions indicates that for the geometry used in our experiments gas phase collisions will increase the measured translational temperature [6], just the opposite of what we observe.

Several other explanations can then be considered for the lower than anticipated translational temperature. Among the possibilities are: (1) energy transfer from translational to internal degrees of freedom; and (2) adiabatic (constant total energy) or near adiabatic desorption from the chemisorption potential energy well. Additionally, trajectory calculations predict that for a nonactivated absorption process, adsorption is weighted toward the low energy

portion of the translational velocity distribution of incident molecules [7]. Microscopic reversibility would then predict desorption of molecules that are cold relative to the thermal bath temperature. The implication of these results is that the CO translational degrees of freedom are not in complete equilibrium with the copper surface heat bath during the desorption process.

Another important result from our previous work was the discovery of a technique for the study of surface diffusion which uses laser induced thermal desorption [1]. A pulsed laser focused to a spot of ~ 1 mm diameter was used to produce thermal desorption of carbon monoxide from a copper surface in ultrahigh vacuum. The desorbed CO was monitored with a quadrupole mass spectrometer. After several pulses occurring within seconds, the region of the surface irradiated by the laser became depleted of adsorbed CO, and the desorption flux reduced to zero. Surface diffusion was studied by observing the time dependence of the recovery of the desorption flux following this initial depletion. To obtain the diffusivity, the desorption flux recovery was fit to the solution of Fick's Law for a circular geometry (see Fig. 3). For CO on a polycrystalline

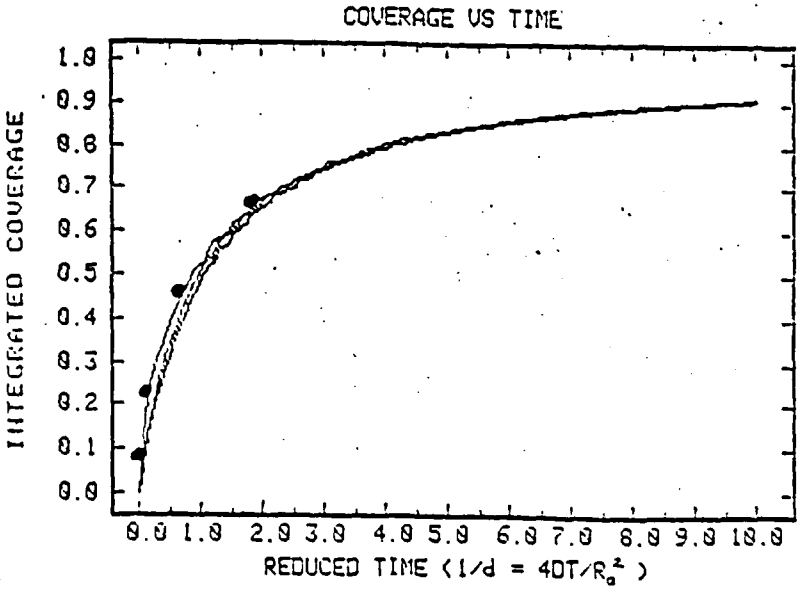

The two solid points correspond to CO diffusion on polycrystaline copper at 90 K. The two open circles are at 110 K. A plot against reduced time shows that these points all fit the appropriate diffusion curve. Initial coverage was saturation coverage of CO. The three different curves show the effect of different laser pulse profiles.

SERS, SERRS and SRRS.

The system components for this apparatus were ordered in November 1979. The main chamber and most of the other components arrived at Northwestern in September 1980. Construction of a functional system was completed by September 1981 and has now been in operation but undergoing continuous refinements since then. Figure 11 shows the layout of the main chamber identifying the equipment located in each port. The main specimen manipulator (including single crystal mount, heating, and cooling capabilities), evaporators, quadrupole mass spectrometer (QMS) mount, gas dosing array (see Figure 12 for details), QXTM (see Figure 13 for electronics details), main optical collection lens in inset port, beam handling optics, and optical relay mirror system were all designed and constructed at Northwestern.

b. SERRS in UHV - Prior to our work, there were no studies of SERRS carried out under UHV conditions. By recognizing that highly purified metallophthalocyanines such as CoPc (see Figure 14) are UHV compatible and support RRS by themselves, we were able to open this new and, so far, unique domain of surface enhanced optical phenomena. We are very excited about the ability to study CoPc and other MPc's under UHV conditions because these are excellent candidates for SERRS as well as SEP studies. Figure 15 shows the first UHV SERRS experiments in which CoPc is evaporated onto clean, cold evaporated Ag at 110° K. We have recorded SERR spectra as a function of coverage. Coverage was determined using AES to measure the N/Ag Auger peak intensity ratio (see Figure 16). We have identified a monolayer and submonolayer coverage region (viz., less than 6 min. deposition at the beam flux used) as well as a multilayer

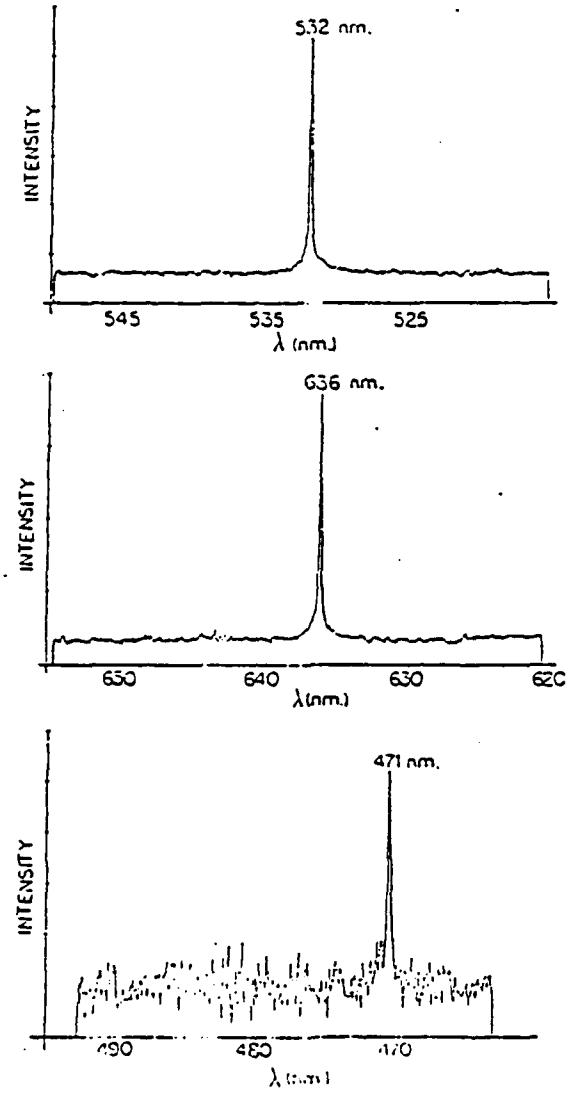

Figure 10. SEHG experiments on roughened Ag electrodes.

TOP PANEL. Surface Enhanced Second Harmonic Generation. Roughened with 200 mC cm^{-2} potential step to +0.20 V vs. SCE in 0.10 M KCl solution. SESHG recorded at solid/electrolyte interface E = 0.0 V vs. SCE. Input laser wavelength = 1.064 microns (viz., Nd:YAG laser fundamental). Laser power = 37.5 KW cm^{-2} corresponding to an un-Q-switched 7.5 mJ pulse. Laser repetition rate = 10 pps. OMA detection used. 180 sec. or data acquisition time.

MIDDLE PANEL. Surface Enhanced Third Harmonic Generation. SETHG recorded at solid/air interface because input laser wavelength = 1.907 microns (viz., 1st Stimulated Raman Stokes shift of 1.064 microns in H_2) is absorbed in water. Laser pulse energy = 1.0 mJ/pulse Q-switched at 10 pps. All other conditions same as top panel.

BOTTOM PANEL. Surface Enhanced Fourth Harmonic Generation. Laser pulse energy = 7 mJ/pulse at 10 pps. 300 sec. of OMA data acquisition time used. All other conditions the same as middle panel.

30-32]. Our Nd:YAG/dye/stimulated Raman laser [10,26] was used as the excitation source. In most experiments the input laser wavelength was 1.907 microns (viz., 1st Stokes shift of 1.06 micron Nd:YAG fundamental in H_2). Since this beam is strongly absorbed by H_2O, the harmonic generation experiments were carried out at the solid/gas (air) interface. No adsorbates were intensionally involved in these experiments. The third harmonic of 1.907 microns is 635.7 nm. and the fourth harmonic is 471 nm. Figure 10 shows these signals along with the second harmonic of 1.06 microns. The intensity of the THG and FHG surface signals is modulated by surface roughness; but, we have not yet quantitatively determined the ROUGH/SMOOTH ratio to our satisfaction. This and the study of SETHG and SEFGH in the presence of adsorbates remains to be done.

e. SERS with Simultaneous Pulsed and CW Laser Excitation - One of our original goals in developing the Nd:YAG/dye/stimulated Raman laser system [10,26] was to be able to use its broad tuning range to be able to more carefully map out SERS excitation profiles [9]. When this was attempted, we found that only 10 microjoules of pulsed laser power could be focussed on SERS-active electrode. Spectra could be obtained in this manner but they required the improved sensitivity detection capabilities of our OMA system. The reason for the low maximum power appears to be laser induced damage of the surface or laser induced (possibly surface enhanced) photochemistry of the adsorbate. We have demonstrated that under appropriate conditions, pyridine is damaged by pulsed laser radiation (532 nm.) by monitoring the CW excited SERS spectrum as a function of the samples exposure to the pulsed laser [25]. Many more experiments need to be done to confirm this result; however, it is possible that this is a

Raman active adsorbate is identical for both experiments [20]. Concurrent SEM studies (see Figure 9) of the roughness show that the size and interparticle spacings of roughness features that optimize the SERS enhancement factor for each metal is DIFFERENT. The conclusions from this work are:

1) Cu and Au are excellent SERS substrates. Since high S/N ratio spectra can be now be obtained, this opens up many more applications for SERS in heterogeneous catalysis and in electrochemistry.

2) One cannot make quantitative judgements about SERS enhancement factors unless they are accompanied at least by roughness characterization measurements AND surface coverage measurements. Furthermore, it would be desirable also to have surface optical absorption measurements to prove that large enhancement factors are or are not simply the result of shifting the adsorbate electronic absorption spectrum into resonance with the laser excitation wavelength as a result of the adsorption chemistry.

3) The electromagnetic particle-plasmon model for the enhancement process is hard pressed to explain the roughness dependence of the SERS enhancement factors that we found in this work.

4) Much more work needs to be done to confirm and generalize these results.

d. SEHG on Ag - In a preliminary study carried out by Dr. Murray Johnston, surface enhanced third harmonic generation (SETHG) and surface enhanced fourth harmonic generation (SEFHG) were discovered [24]. These experiments were carried out on Ag samples electrochemically anodized in the usual way

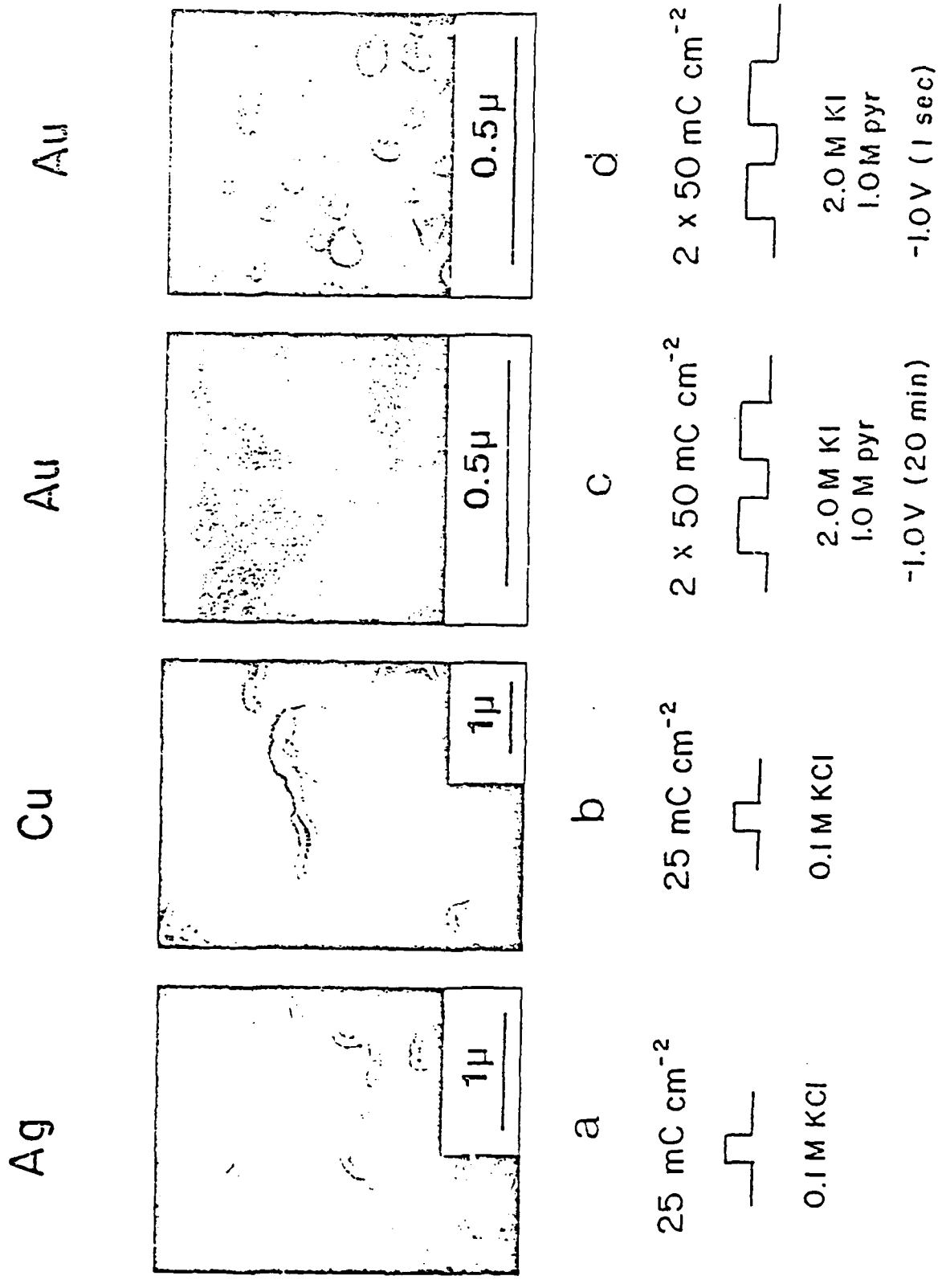

Figure 9. Scanning electron micographs of the roughened electrodes used in the SERS experiments of Figure 8. Particularly note the comparison between surfaces c and d. Both surfaces c and d are gold and are roughened IDENTICALLY. The only difference is the length of time the potential is held at -1.0 V vs. SCE prior to electrode disconnect and SEM observation. Electrode c is SMOOTHER than electrode d, yet the

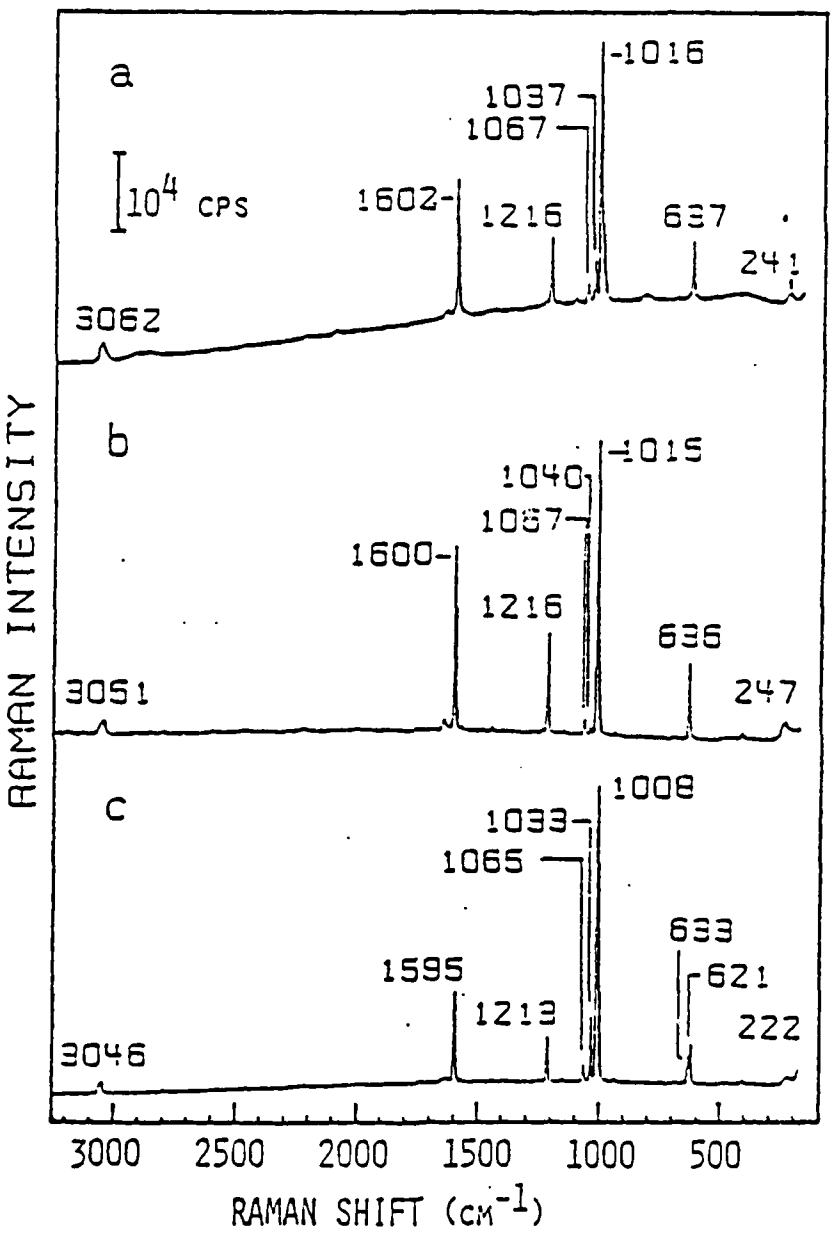

Figure 8. SERS of pyridine on Ag, Cu and Au electrodes. DIFFERENT surface roughening conditions used for the GOLD electrode as compared to Figure 7A. Laser wavelength = 647.1 nm.

A. Au electrode. Anodized with two 50 mC cm^{-2} steps to +0.19 vs. SCE in 2.0 M KI/1.0 M pyridine solution. SERS recorded at E = -1.0 V vs. SCE. Laser power = 100 mW. EF = 5.9 x 10^6.

B. Cu electrode. All conditions the same as Figure 7B.

C. Ag electrode. All conditions the same as Figure 7C.

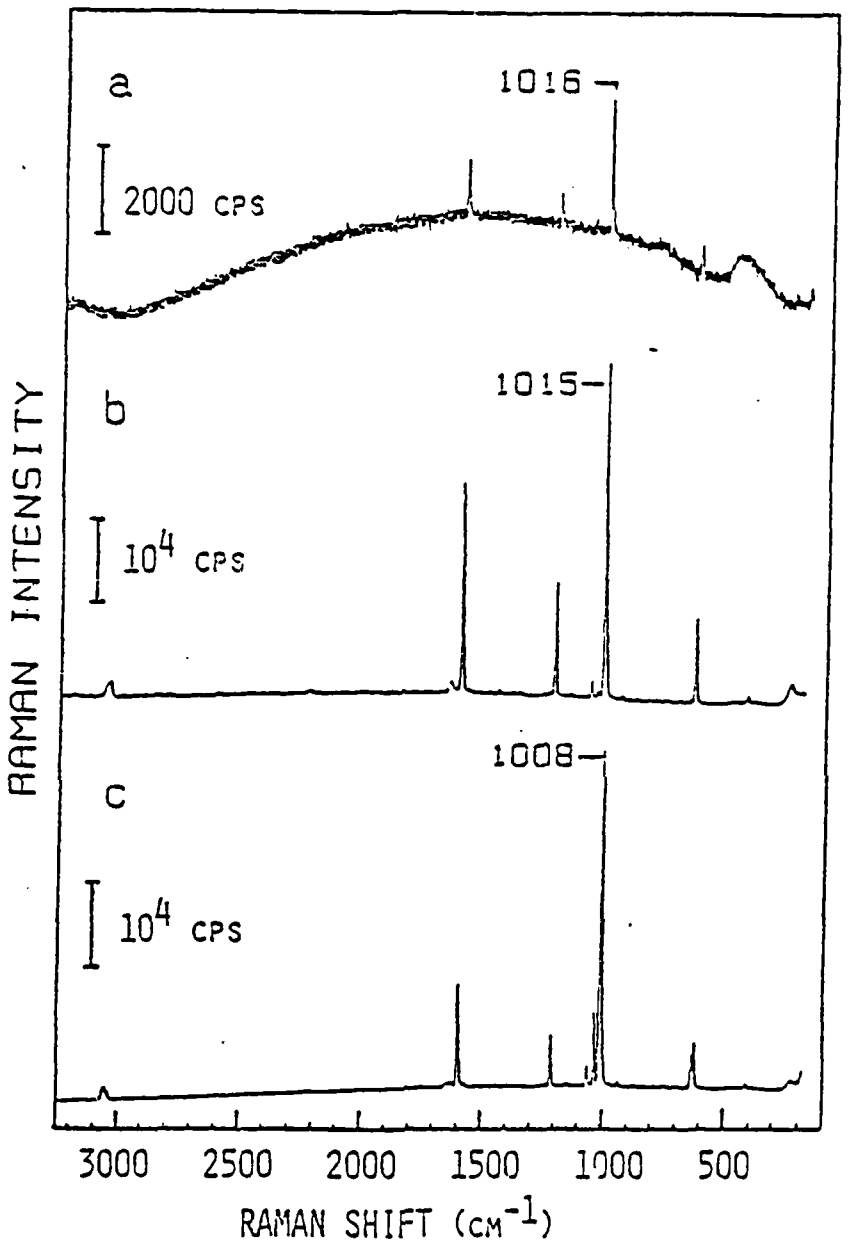

Figure 7. SERS of pyridine adsorbed on Ag, Cu and Au electrodes. Laser wavelength = 647.1 nm.

A. Au electrode. Anodized with two 25 mC cm^{-2} steps to +1.3 V vs. SCE. in 0.10 M KCl/0.05 M pyridine solution. SERS recorded at E = -0.85 V vs. SCE. Laser power = 100 mW. EF = 10^4.

B. Cu electrode. Anodized with one 25 mC cm^{-2} step to -0.05 V vs. SCE in 0.10 M KCl/0.05 M pyridine solution. SERS recorded at E = -0.85 V vs SCE. Laser power = 20 mW. EF = 2.9×10^6.

C. Ag electrode. Anodized with one 25 mC cm^{-2} step to +0.19 V vs. SCE in 0.10 M KCl/0.05 M pyridine solution. SERS recorded at E = -0.85 V vs. SCE. Laser power = 20 mW. EF = 2.9×10^6.

growth of the intensity of 1011 cm^{-1} Raman line of the complex with time. Similarly, the total charge passed at the electrode, which is a measure of the number of moles of Cd^{+2} generated, is a linear function of time (see Figure 6B). The charge passed at the end of 200 seconds is equivalent to 2000 monolayers of the complex. This result again demonstrates the great importance of making coverage measurements along with surface Raman measurements in order to be sure that simple multilayer formation is not responsible for apparent enhancement.

c. Quantitative Enhancement Factors for SERS on Ag, Cu and Au - It is widely believed that the INTRINSIC values for the SERS enhancement factors for pyridine on Ag, Cu and Au scale in the order Ag = 10^6, Cu = 10^5, and Au = 10^4. This is based both on electrochemical [19] and UHV [20] SERS results. Recently we have carried out a series of experiments designed to test this assertion and have found one set of electrochemical SERS conditions (see Figure 4) under which the SERS enhancement factors for pyridine adsorbed on Ag, Cu and Au do scale in the order Ag = 1 x 10^6, Cu = 1 x 10^5 and Au = 1 x 10^4 and another set of conditions (see Figure 5) under which they scale in the order Ag = 2.9 x 10^6, Cu = 2.9 x 10^6, and Au = 5.9 x 10^5 [19] and [20]. In other words, we have found NEW conditions under which Cu has the SAME ENHANCEMENT FACTOR as Ag and Au is ONLY A FACTOR OF 5 WEAKER than either Ag or Cu. The only difference between these two experiments is the method of roughening the surface. For the experiments shown in Figure 7, all electrodes were anodized (i.e. roughened) IDENTICALLY; whereas, the experiments depicted in Figure 8 involved electrodes that were roughened in DIFFERENT solutions. Parallel studies of surface coverage using the technique of double potential step chronocoulometry show that the surface concentration of

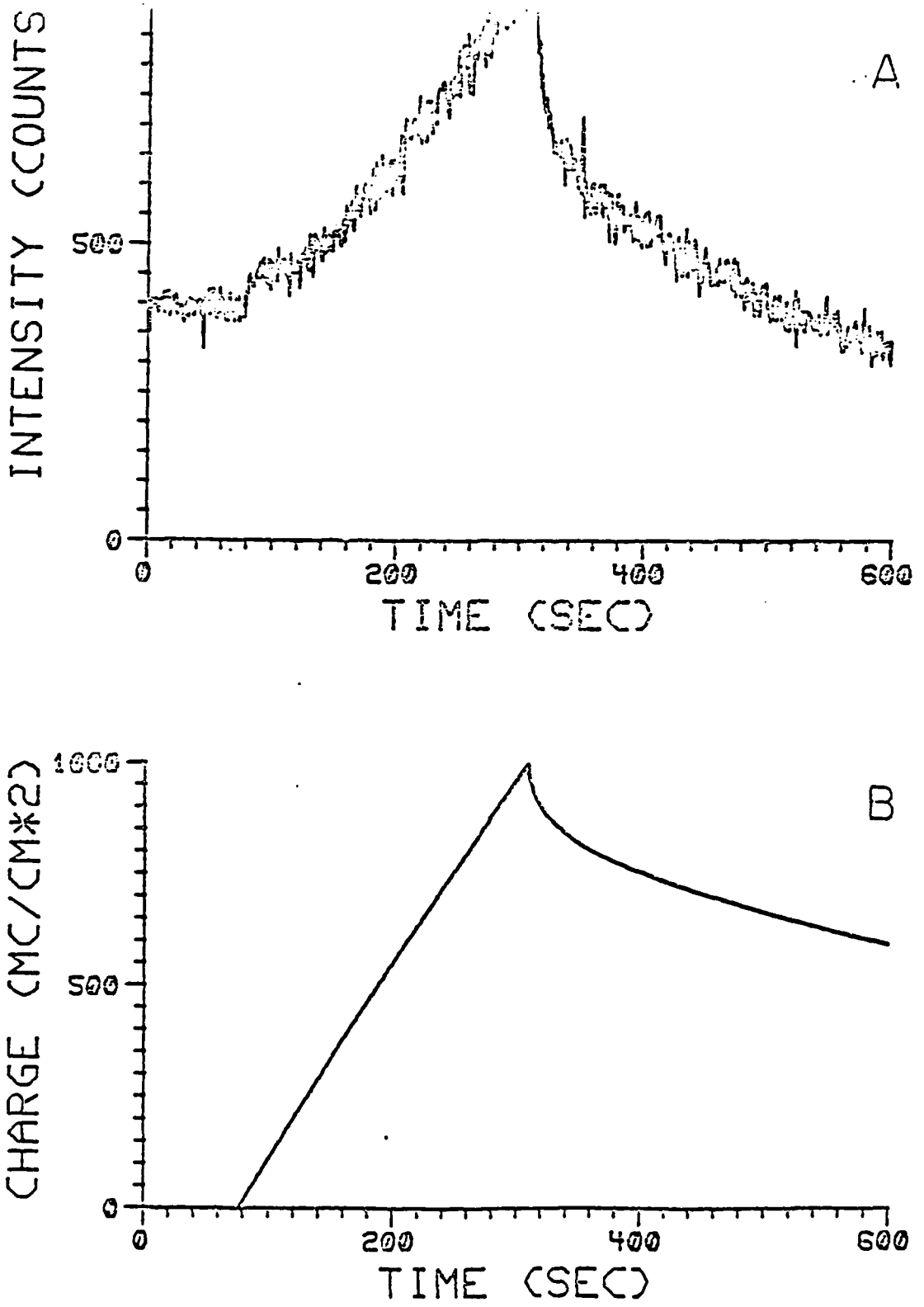

Figure 6. A. Raman intensity of 1011 cm^{-1} line in Figure 4B vs. time. This transient was initiated by a potential step originating at -1.3 V then stepping to -0.6 V to generate Cd+2 and terminating at -1.3 V which reduces the $CdCl_2$ 2Py complex. Laser wavelength = 514.5 nm. Laser power = 50 mW.

B. Charge passed in electrochemical cell during the Raman transient experiment of Figure 6A. The charge at the peak of the transient corresponds to 2000 monolayers of $CdCl_2$ 2Py.

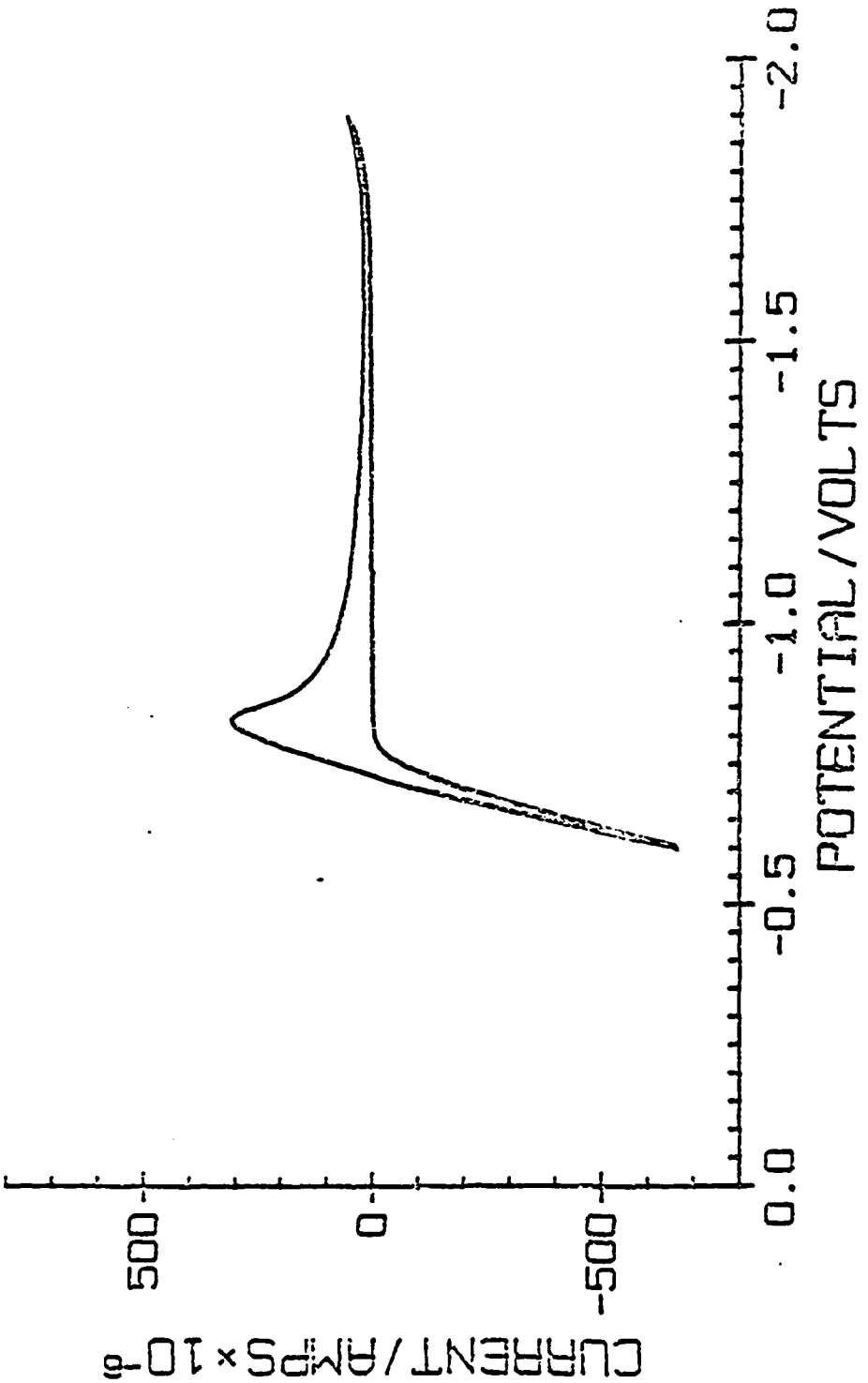

Figure 5. Cyclic voltammogram of a Cd metal electrode in 0.10 M KCl/0.05 M pyridine solution. Note that at E = -0.70 V vs. SCE, the potential at which the Raman spectrum shown in Figure 4B was recorded, Cd+2 ion is being generated (i.e. a finite oxidation current is flowing).

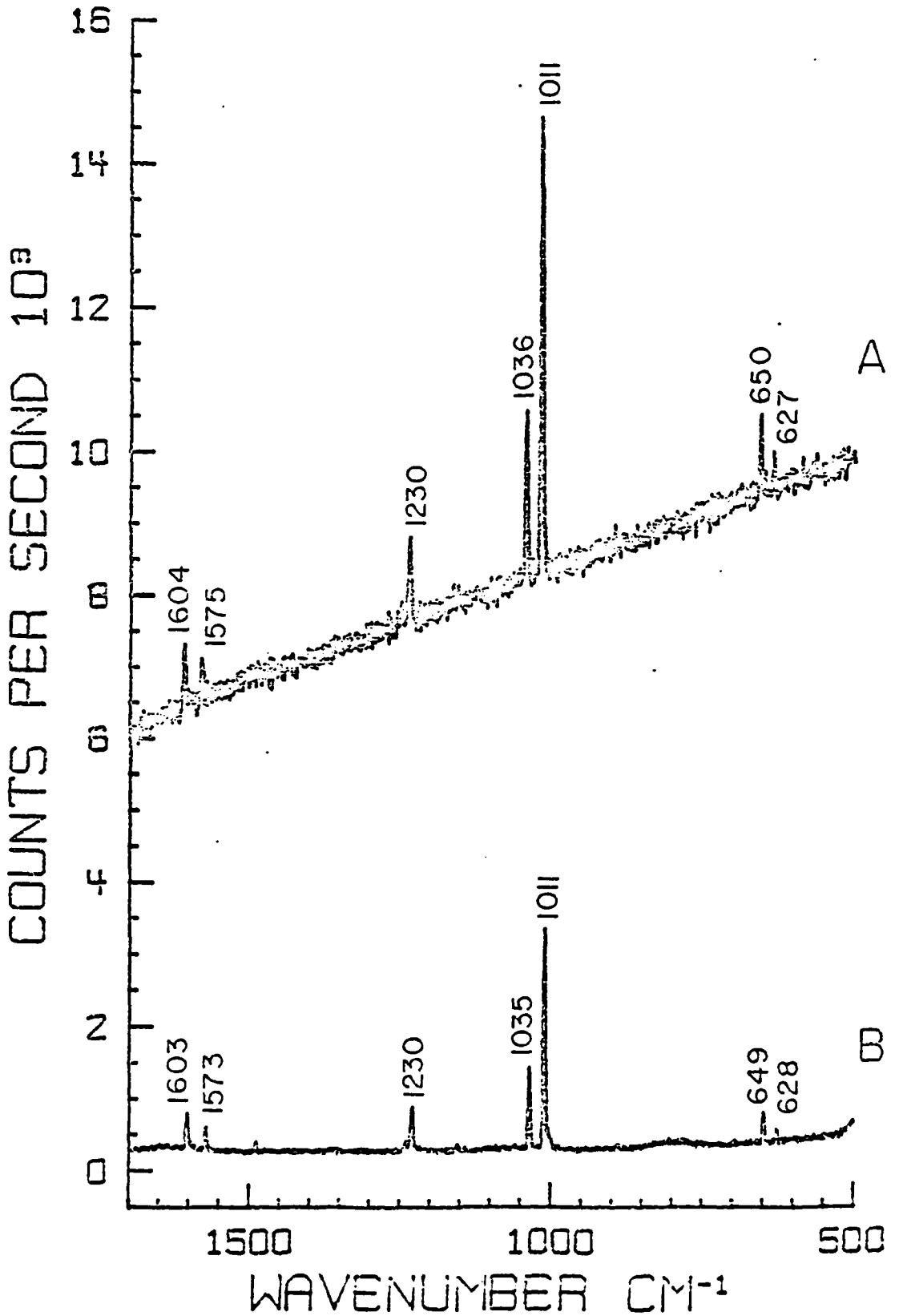

Figure 4. A. Normal Raman spectrum of $CdCl_2 \cdot 2Py$. Laser wavelength = 647.1 nm. Laser power = 10 mW.

B. Supposed SERS of pyridine on Cd metal electrode [20]. 0.1 M KCl/ 0.05 M pyridine solution. E = -0.7 V vs. SCE. Laser wavelength = 647.1 nm. Laser power = 100 mW.

tors that are as large as those from intermediate sized organic molecules such as pyridine. In addition the high symmetry of these complexes allows us to assign the adsorption geometry using symmetry lowering effects of adsorption on multiple degenerate vibrational bands. The particular complexes studied were $Fe(o\text{-phen})_3^{2+}$ [14]; $Cd(SCN)_4^{-}$ [15]; MoO_4^{-} and $Pt(CN)_4^{-}$ [16]; on Ag [14,16] and Cu [16] electrodes. All of this work is similar in character and in general conclusions to our work on $Ru(CN)_6^{-4}$ [12]. coverage measurements were made on $Cd(SCN)_4^{-}$ by DPSCC [17] and prove that less than 1 monolayer of complex is present under conditions where the corresponding SERS experiments were carried out [15].

b. SERS on Substrates Other Than Ag, Cu and Au - One of our overall objectives has been to determine the extent to which substrates other than Ag, Cu, and Au possess enhancement properties. Recently Loo reported that Cd metal shows strong SERS for adsorbed pyridine under electrochemical conditions [27]. We have reinvestigated this system and conclude [23]:

1) Loo's pyridine on Cd spectrum can be reproduced

2) The spectrum reported in [27] is NOT A TRUE SERS SIGNAL

Figure 4 shows that a spectrum identical to the one reported by Loo at -0.6 to -0.8 V on Cd can be obtained by synthesizing a cadmium-chloride-pyridine complex, $CdCl_2 \cdot 2$ pyr. The cyclic voltammogram in Figure 5 shows that at all applied potentials where the pyridine on Cd Raman spectrum can be observed (viz., potential positive of -0.8V), Cd^{+2} is being electrogenerated. Cd^{+2} then reacts with solution phase Cl^- and pyridine to form a multilayer of $CdCl_2 \cdot 2$pyr. on the electrode. This is demonstrated in Figure 6A by the linear

III. Surface Enhanced Optical Spectroscopy

The primary goals of this research were to investigate the fundamental mechanisms underlying Surface Enhanced Raman Spectroscopy (SERS) and related techniques, and to explore the substrate and molecular generality of surface enhanced spectroscopic methods.

A. Experiment

Our experimental work under the ONR contract was concerned with various fundamental aspects of SERS, SERRS (Surface Enhanced Resonance Raman Scattering), and SEHG (Surface Enhanced Harmonic Generation). Papers published, in press, or submitted as a results of this work include Refs. 8-26 in the list of references. These research accomplishments are in the areas of: 1) electrochemical SERS, SERRS, and SEHG studies; 2) UHV SERS, SERRS, and RRS studies; and 3) SERRS and fluorescence quenching studies at solid/gas interfaces.

1. Electrochemical SERS, SERRS and SEHG Studies

Refs. 8-26 deal with a number of different aspects of surface enhanced optical spectroscopy in electrochemical environments, including: a) adsorbate generality of SERS [14-17]; b) SERS on substrates other than Ag, Cu, and Au [14,23]; c) quantitative enhancement factors for SERS on Ag, Cu, and Au combined with surface roughness characterization and coverage measurements [19,20]; d) SEHG on Ag [24]; and e) SERS with simultaneous pulsed and CW laser excitation [25].

a. Adsorbate Generality of SERS - Our work in this area [14-17] clearly demonstrates that transition metal coordination complexes show enhancement fac-

copper surface at 85 K the diffusivity was determined to be 5×10^{-7} cm^2 sec^{-1}.

This technique offers a number of advantages over previous methods. Perhaps the most important is that it can be applied to any adsorbate which thermally desorbs cleanly from a surface. The laser beam is apertured so that the boundary of the irradiated area is sharp. The time duration of the laser pulses (15 nanoseconds) as well as the recovery time for the surface temperature to return to ambient (~ 100 nanoseconds as estimated by time resolved black body emission) are fast compared to diffusion times which are on the order of seconds. Therefore, diffusion during the pulse should not cause significant spreading of the adsorbate boundary and a sharply defined initial concentration gradient can be formed without an elaborate masking procedure. The directional anisotropy of diffusion can be probed by using an oriented line focus for the incident laser radiation instead of a spot focus. In addition to the usual equipment needed for surface preparation and characterization, the only additional requirement is a pulsed laser with sufficient energy to desorb the surface species of interest. In our initial experiments a mass spectrometer was used to detect desorption, but the signals are large enough that an ion gauge would serve just as well for many experiments.

VALID CASE OF SEP. Concurrent SEM studies have not yet been done to check on the extent of laser induced damage to the surface roughness.

2. UHV SERS, SERRS and SRRS Studies

The accomplishments in this area deal with three topics: a) construction of a versatile UHV sample preparation/surface enhanced optical spectroscopy/electron and particle spectroscopy system; b) measurement of the first SERRS spectrum in UHV and determination of the incremental enhancement factor between SRRS and SERRS [33]; and c) a comparative study of SERS for the pyridine/Cl^-/Ag system in UHV and electrochemical environments [29].

a. Construction of UHV Apparatus - One of the major activities of the grant period has been the construction of a very versatile UHV optical and electron spectroscopy system capable of:

1) UHV sample preparation including ion bombardment cleaning; sample temperature control from 90°K to 1500°K by LN2 cooling and e-beam heating; in situ evaporation of 2 different SERS active metals, metallophthalocyanines, or CaF_2 onto a single crystal substrate; and back filling the chamber with volatile adsorbates through a leak valve.

2) Measuring the coverage of an adsorbate by either dosing the crystal directly with a known number of molecules in a microchannel plate array doser or using quartz crystal thickness monitor (QXTM) techniques.

3) Determining the atomic composition and structure of the surface by AES, XPS and LEED techniques.

4) Determining the vibrational spectroscopic properties of the surface by

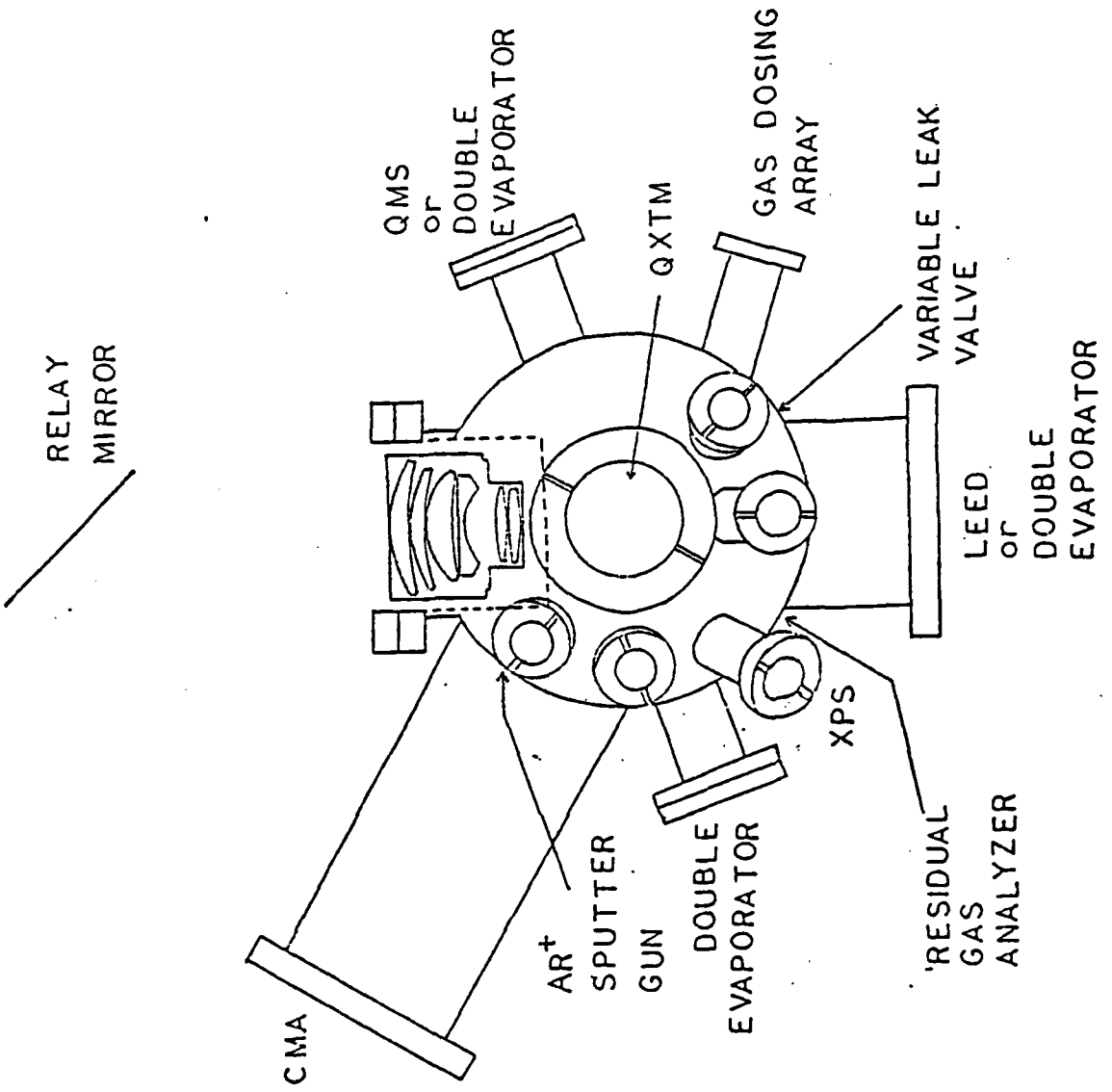

Figure 11. UHV/SERS/Electron Spectroscopy Apparatus.

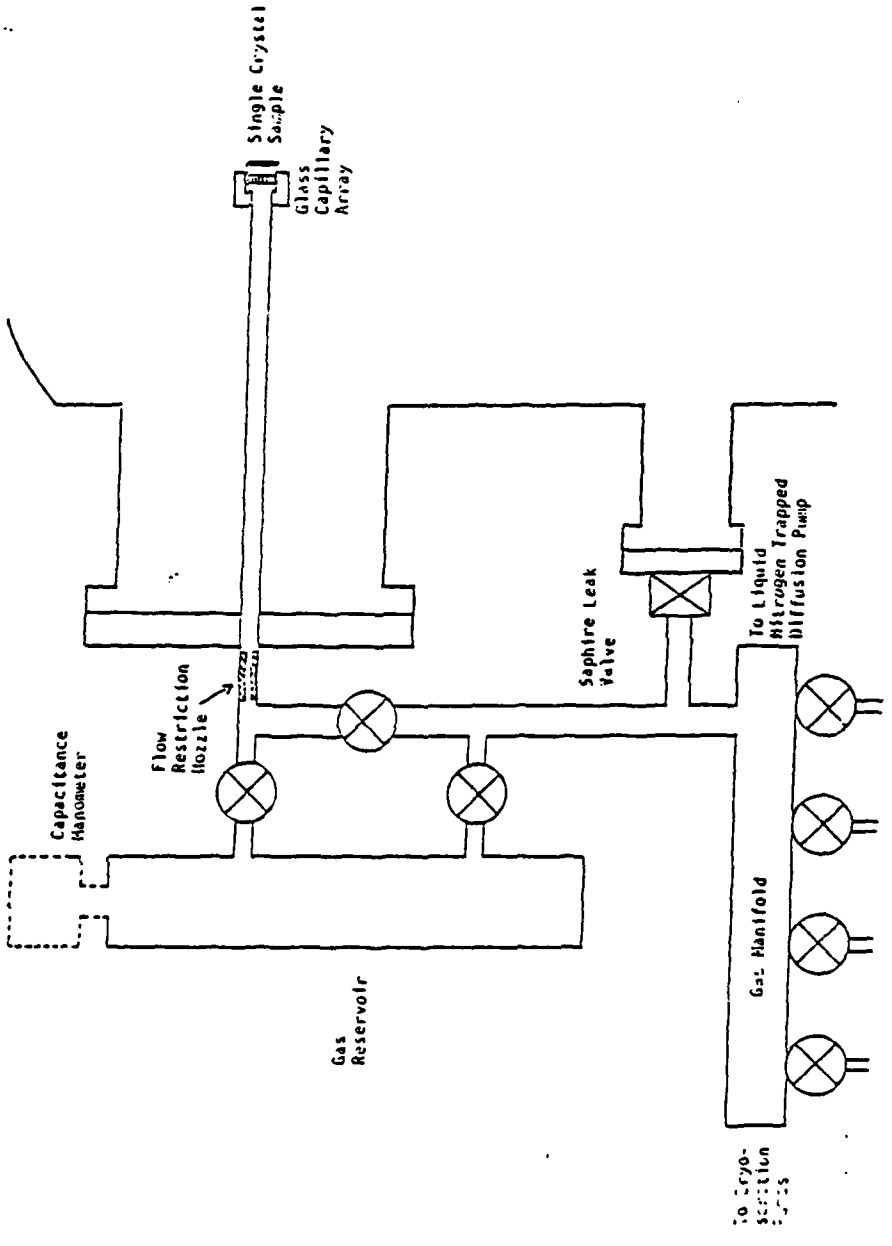

Figure 12. Microchannel plate array adsorbate doser. The capcitance manometer shown in dotted lines is requested in the capital equipment budget of this proposal.

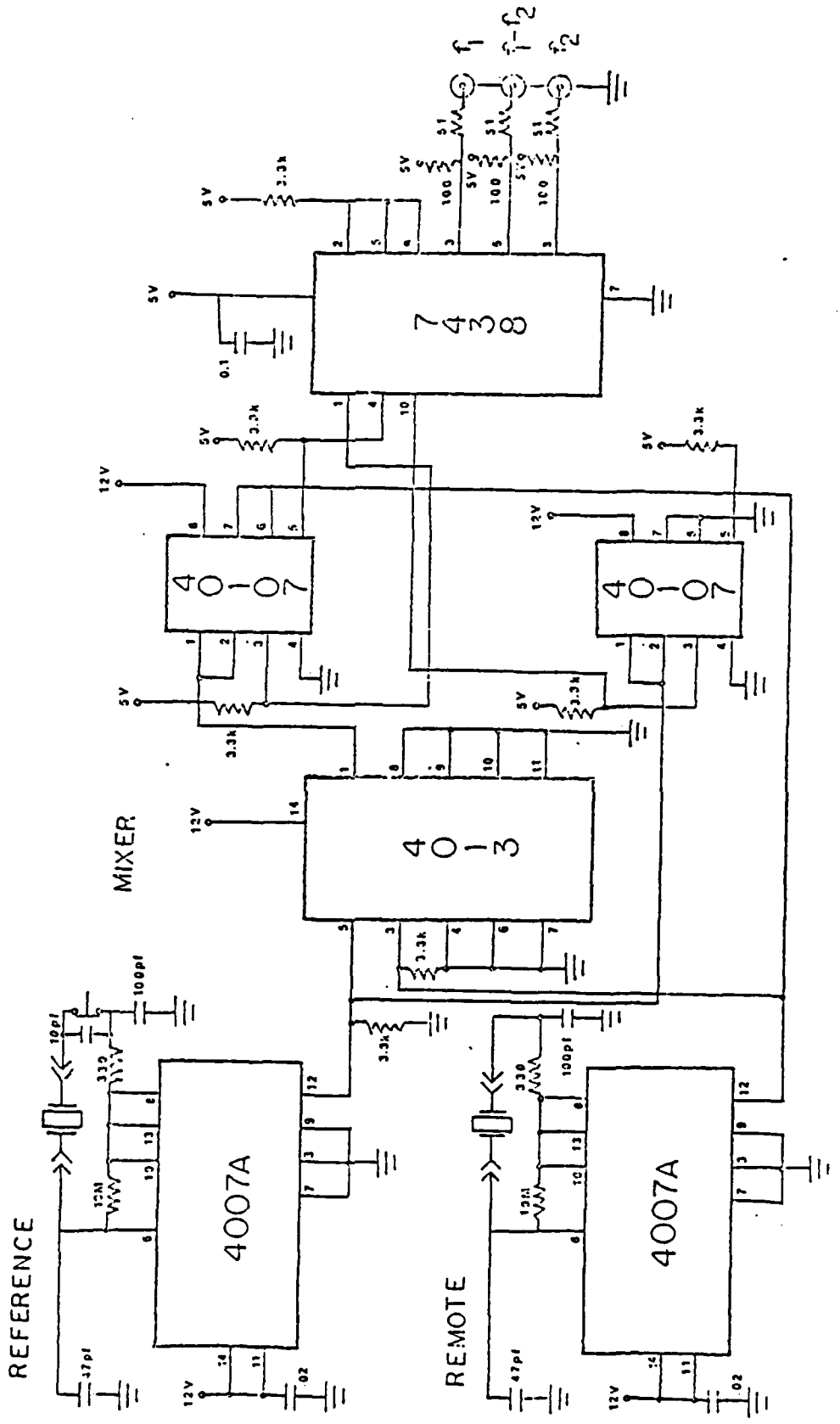

Figure 13. Circuit details for the QXTM readout. Adapted and Modified from the circuit of Ashworth and Snacklette in Rev. Sci. Inst. 49, 1653 (1978).

COBALT PHTHALOCYANINE

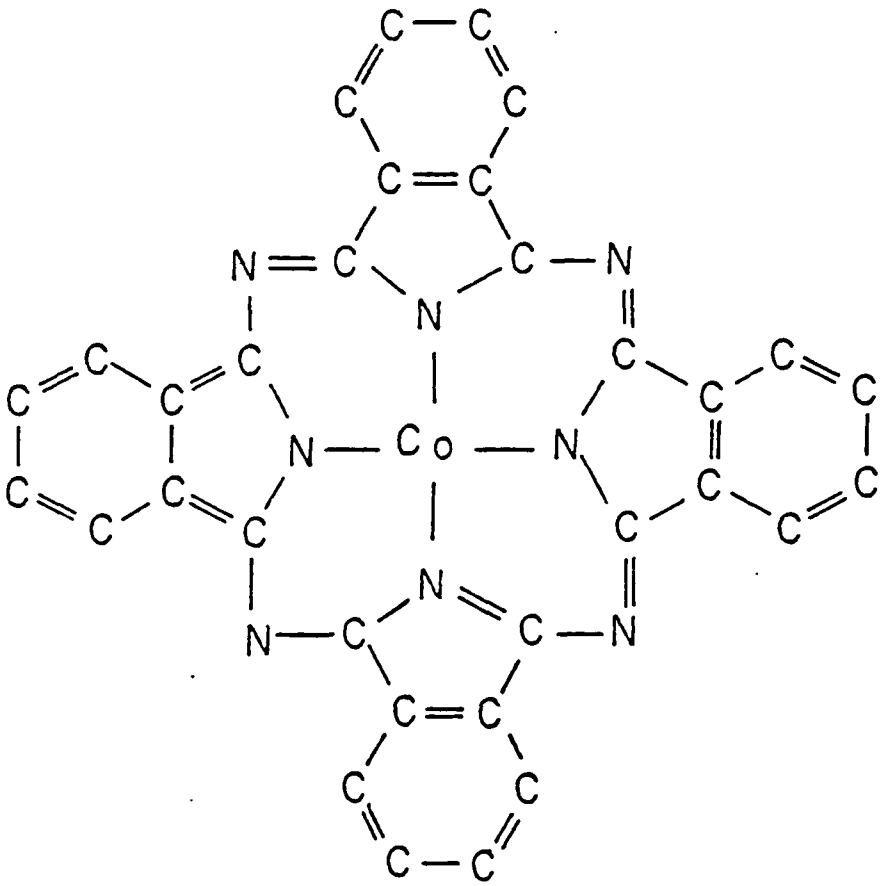

1) Sublimes near 650K - UHV compatible

2) Absorbs near 660 nm ($\epsilon = 10^5$ cm^{-1}) - SERRS

3) Interacts weakly with surface

4) LEED patterns can be obtained

Figure 14. Structure and UHV SERRS properties of CoPc.

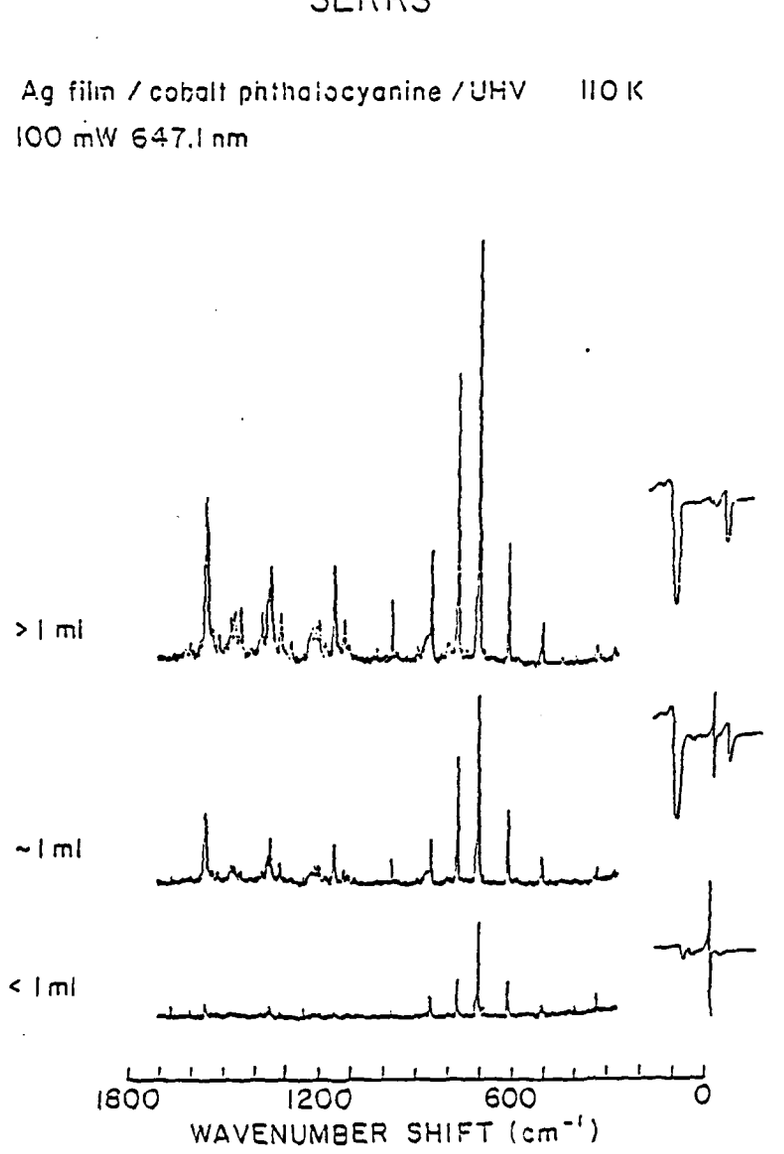

Figure 15. UHV SERS of CoPc on Cold Evaporated Ag film in UHV

TOP PANEL. Multilayer CoPc

MIDDLE PANEL. 1 monolayer of CoPc

BOTTOM PANEL. submonolayer CoPc

Auger spectra of CoPc on Ag are shown to the right of each SERRS. The 3 main AES lines are (from right to left) C, Ag, N.

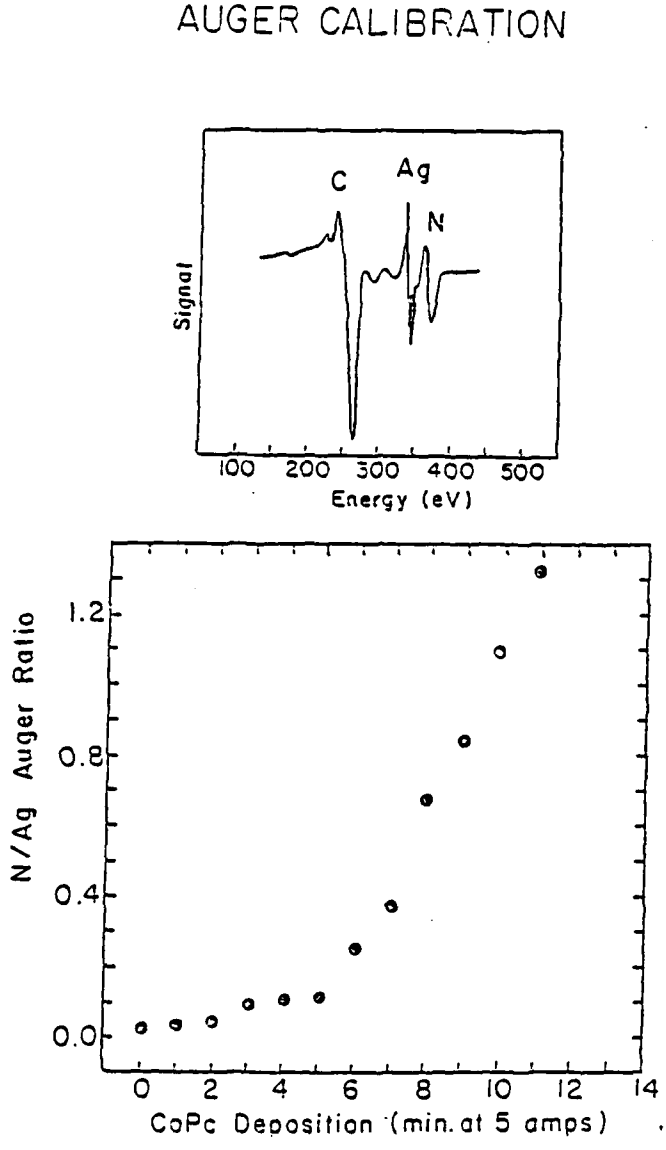

Figure 16. Coverage of CoPc on Ag by Measurement of AES N/Ag peak ratio. The top panel SERRS in Figure 15 was taken at a coverage corresponding to a 10 min. CoPc deposition at 5 amps. The middle panel SERRS in Figure 15 was taken at a coverage corresponding to a 4 min. CoPc deposition at 5 amps. The bottom panel SERRS in Figure 15 was taken at a coverage corresponding to a 2 min CoPc deposition at 5 amps.

region. Strong SERR spectroscopic differences between these two regions are easily seen in the excellent S/N ratio spectra shown in Figure 15 SERR intensity has been studied as a function of Ag film temperature history (viz., annealing experiments). In addition the co-deposition of pyridine and CoPc has been studied. The ligation reaction between pyridine has been observed as well as situations where pyridine and CoPc coexist on the surface as separate molecular entities.

c. SERS of the Pyridine/Cl^-/Ag System in UHV and Electrochemical Environments - Since this chemical system has become the de facto model system for SERS, we felt that a particularly important application of the new UHV SERS apparatus would be to study the same adsorbate/substrate system in the same laboratory and on the same apparatus under UHV and electrochemical conditions. Figure 17 compares SERS in electrochemical and UHV environments. This data shows that: 1) surfaces prepared carefully under electrochemical conditions do NOT show spectroscopic features indicative of carbonaceous layers; 2) coadsorbed counterions such as Cl^- do lead to spectroscopically observable differences in the Raman intensity pattern; and 3) SERS signals observed in UHV are inherently weaker than in electrochemical environments.

3. SERRS and Fluorescence Quenching Studies at Solid/Gas Interfaces

The work carried out in this area parallels and is complimentary to that done on SERRS in UHV. We have been primarily concerned with the SERRS and fluoresence quenching phenomena associated with specimens that we call thin metal film/molecular layer assemblies (TMF/MLA) [18]. TMF/MLA's are fabricated

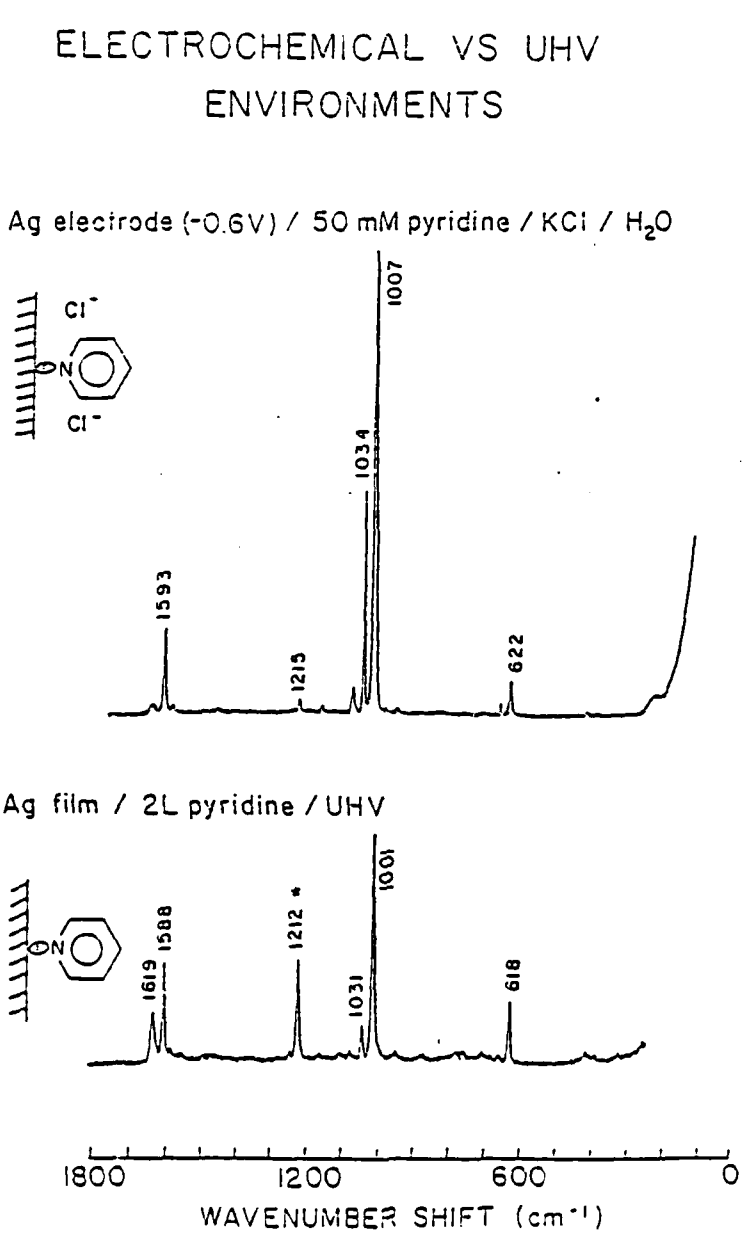

Figure 17. Comparison of SERS in Electrochemical and UHV environments. Laser wavelength = 647.1 nm. Laser power = 10 mW.

by vacuum deposition (viz., conventional oil diffusion pumped chamber at ca. 10^{-6} torr) of SERS-active metals (viz., Ag, Cu and Au) onto glass, quartz, semiconductor, etc. substrates. The surface roughness of these films is controlled by the temperature of the substrate, the nature of the substrate, the rate of deposition, the thickness of the metal film, etc. In some cases the surface of the substrate has been modified by predepositing a CaF_2 layer or a polymer layer to change the roughness characteristics of the substrate and the film deposited on it. The next stage of TMF/MLA fabrication involves the deposition of a molecular layer which may range in thickness from 0.001 monolayer to 1000 monolayers. In our experiments we have concentrated on molecular layers composed of SERRS-active molecules and/or HIGHLY FLUORESCENT MOLECULES. The specimen fabrication procedure described so far would be termed a single layer TMF/MLA. Multilayer assemblies are prepared by evaporating other SERS-active metal and/or molecular layers over the first. Multilayer specimens that involve a SERS metal underlayer/a molecular middle layer/and a SERS metal overlayer are described as "sandwiches." SERRS experiments are carried out by mounting the TMF/MLA on a spinning sample holder and backscattering the laser from its surface. Thus these are Solid/Gas (air) interfacial experiments.

The great advantage of TMF/MLA experiments is that, unlike UHV experiments, one can survey many specimens per unit time and systematically study the effects of substrate structure (viz., single crystal vs. polycrystalline substrate), roughening film (CaF_2 or polymer), SERS metal underlayer morphology (viz.,island film, cold evaporated film, continuous film, particulate film), molecular layer identity and thickness, and SERS metal overlayer morphology. During the past 18 months we have carried out exploratory experiments to define the experimental

observables and have developed the capabilities for preparation of TMF/MLA's and the measurement of the various film thicknesses. At the present time we are systematically studying the effects of all sample fabrication variables on the SERRS observables.

Figures 18 and 19 show representative examples of THF/MLA for several molecules which are normally extremely FLUORESCENT (viz., the laser dye Rhodamine 6G (R6G), acridine orange (AO), Chlorophyll a (Chl a), and Flavin mononucleotide (FMN); and, therefore, cannot be studied by any spontaneous Raman scattering method. Vibrational spectra for these molecules have been obtained, at least over limited cm^{-1} ranges and with substantial experimental complexity, using coherent Raman techniques such as resonance CARS and resonance inverse Raman scattering. The most striking feature of these TMF/MLA SERR spectra is that by control of surface roughness at the metal/molecule interface we can BOTH ENHANCE RRS AND QUENCH FLUORESCENCE. This is an extremely important result in that it should allow us to carefully study the competition between RRS enhancement and fluorescence enhancement or quenching as a function of all specimen preparation variables. Furthermore, these samples are stable in a gas phase environment, provide excellent sensitivity (we have now detected high S/N ratio spectra for 0.001 monolayers of CoPc), should allow us to carry out very meaningful studies of heterogeneous catalytic phenomena, and rapidly screen systems for more detailed characterization in UHV.

As mentioned above we have developed appropriate methodology for measuring the quantitative aspects of these TMF/MLA SERR spectra. Metal film thicknesses can now be measured in our laboratory over the 0.5 - 500 nm range by: 1)QXTM techniques; 2) electrochemical methods such as stripping voltammetry of the Ag,

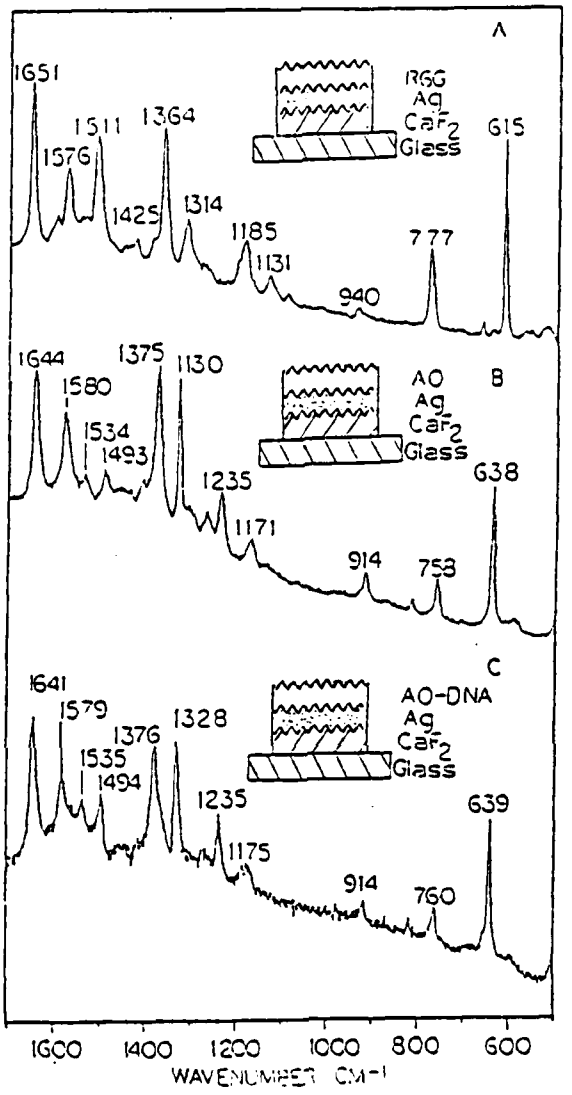

Figure 18. SERRS of Fluorescent Dye Molecules on CaF_2 Roughened Ag Films.

A. Rhodamine 6G. R6G was spin coated from 5 x 10^{-4} M Methanol solution onto a CaF_2 roughened Ag film supported on glass. The Ag film was vapor deposited at 10^{-5} torr and is ca. 200 nm thick. Laser wavelength = 514.5 nm. Laser power = 10mW. Slit width = 3 cm^{-1}. Scan rate = 60 cm^{-1}.

B. Acridine Orange. AO was spin coated from a 5 x 10^{-4} M aqueous buffer (pH = 4.9) onto the same type of roughened Ag film as in A. Laser wavelength = 488.0 nm. Laser power = 10 mW. Slit width = 4 cm^{-1}. Scan rate = 60 cm^{-1}/min.

C. Acridine Orange bound to DNA. AO-DNA spin coated from a saturated DNA/AO solution. All other conditions are the same as B.

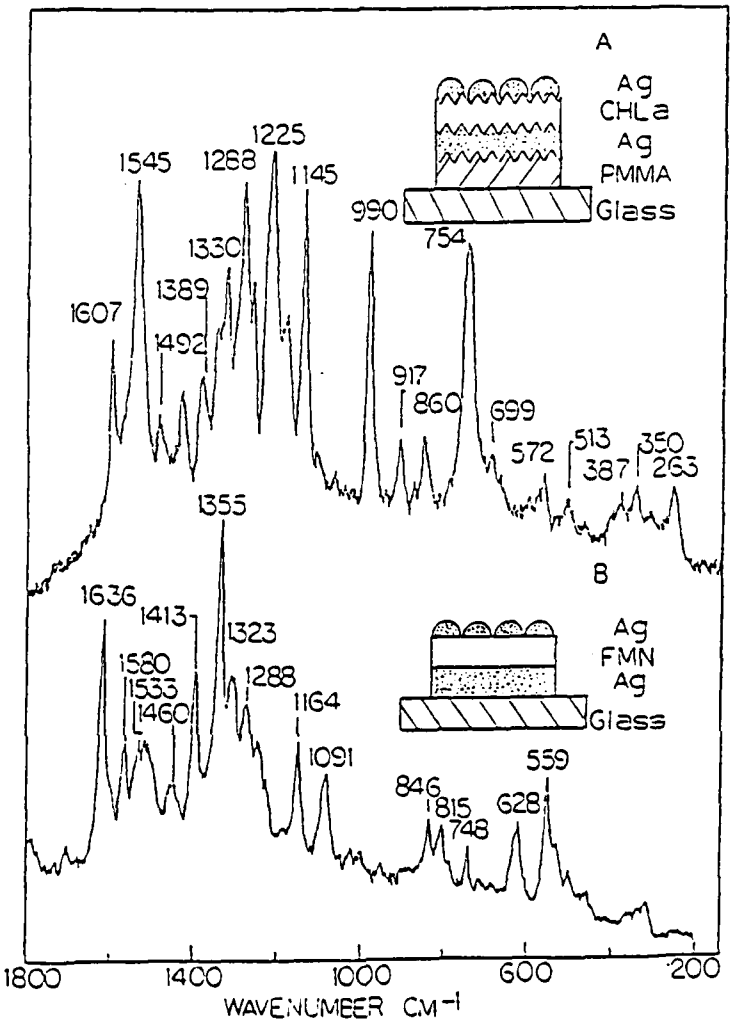

Figure 19. SERRS of Fluorescent Biological Molecules in Thin Metal Film/Molecular Layer Assemblies.

A. Chlorophyl a. CHla was spin coated from a 10^{-3} M pyridine solution on to a polymethylmethacrylate (PMMA) roughened Ag film supported on glass. The PMMA was spin coated onto the glass and then overcoated with a 200 nm. Ag film by vapor deposition at 10^{-5} torr. This assembly was then overcoated again with a Ag island film of ca. 5 nm. mass thickness. Laser wavelength = 647.1 nm. Laser power = 50 mW. Slit width = 3 cm^{-1}. Scan rate = 60 cm^{-1}/min.

B. Flavin Mononucleotide. FMN was spin coated from a 10^{-3} M nexane solution on to a smooth Ag film (ca. 200 nm. thick) vapor deposited on glass. After FMN deposition this TMF/MLA was overcoated with a 5 nm Ag island film. Laser wavelength = 514.5 nm. Laser power = 20 mW. Slit width = 3 cm^{-1}. Scan rate = 60 cm^{-1}/min.

Cu, or Au film from carbon electrodes placed in the deposition chamber; and 3) atomic absorption spectroscopy or electrochemistry of Ag, Cu, and Au solutions prepared by dissolution of test films in acidic solutions. Molecular layer thicknesses are determined by conventional absorption spectroscopy following dissolution of known area test films (viz., dissolve CoPc in pyridine solutions and measure the resulting uv-vis absorption spectrum). Systematic experiments are now in progress to measure the SERRS enhancement factor as a function of molecular coverage and metal film thickness to yield a 3-D surface that defines the optimum sensitivity of this spectroscopy. It is safe to say at this time that optimized SERRS is the most sensitive vibrational spectroscopy so far discovered.

B. THEORY

Our theoretical work under the ONR contract was been directed towards understanding surface enhanced Raman scattering (SERS). Papers published as a result of this work include Refs. 9, 34-40. These papers (and the research done) may be divided into three broad categories: (a) phenomenological studies of simple SERS models [Refs. 9, 34 and 36], (b) a detailed evaluation of local field enhancements arising from randomly roughened surfaces [papers 35 and 37], and (c) *ab initio* calculations of SERS intensities [papers 38, 39 and 40]. Since paper [36] is a review article of our work on simple SERS models, we will refer the interested reader to that paper for a discussion of our work in that category. Our accomplishments under (b) and (c) are summarized in the following paragraphs.

TECHNICAL REPORT DISTRIBUTION LIST, 359

	No. Copies
Dr. H. Richtol Chemistry Department Rensselaer Polytechnic Institute Troy, New York 12181	1
Dr. A. B. Ellis Chemistry Department University of Wisconsin Madison, Wisconsin 53706	1
Dr. M. Wrighton Chemistry Department Massachusetts Institute of Technology Cambridge, Massachusetts 02139	
Larry E. Plew Naval Weapons Support Center Code 30736, Building 2906 Crane, Indiana 47522	1
S. Ruby DOE (STOR) 600 E Street Providence, Rhode Island 02192	1
Dr. Aaron Wold Brown University Department of Chemistry Providence, Rhode Island 02192	1
Dr. R. C. Chudacek McGraw-Edison Company Edison Battery Division Post Office Box 28 Bloomfield, New Jersey 07003	1
Dr. A. J. Bard University of Texas Department of Chemistry Austin, Texas 78712	1
Dr. M. M. Nicholson Electronics Research Center Rockwell International 3370 Miraloma Avenue Anaheim, California	1
Dr. R. P. Van Duyne Department of Chemistry Northwestern University Evanston, Illinois 60201	
Dr. B. Stanley Pons Department of Chemistry University of Alberta Edmonton, Alberta CANADA T6G 2G2	
Dr. Michael J. Weaver Department of Chemistry Michigan State University East Lansing, Michigan 48824	
Dr. R. David Rauh EIC Corporation 55 Chapel Street Newton, Massachusetts 02158	
Dr. J. David Margerum Research Laboratories Division Hughes Aircraft Company 3011 Malibu Canyon Road Malibu, California 90265	
Dr. Martin Fleischmann Department of Chemistry University of Southampton Southampton SO9 5NH England	
Dr. Janet Osteryoung Department of Chemistry State University of New York at Buffalo Buffalo, New York 14214	
Dr. R. A. Osteryoung Department of Chemistry State University of New York at Buffalo Buffalo, New York 14214	

TECHNICAL REPORT DISTRIBUTION LIST, 359

	No. Copies
Dr. Paul Delahay Department of Chemistry New York University New York, New York 10003	1
Dr. E. Yeager Department of Chemistry Case Western Reserve University Cleveland, Ohio 41106	1
Dr. D. N. Bennion Department of Chemical Engineering Brigham Young University Provo, Utah 84602	1
Dr. R. A. Marcus Department of Chemistry California Institute of Technology Pasadena, California 91125	1
Dr. J. J. Auborn Bell Laboratories Murray Hill, New Jersey 07974	1
Dr. Adam Heller Bell Laboratories Murray Hill, New Jersey 07974	1
Dr. T. Katan Lockheed Missiles and Space Co., Inc. P. O. Box 504 Sunnyvale, California 94088	1
Dr. Joseph Singer, Code 302-1 NASA-Lewis 21000 Brookpark Road Cleveland, Ohio 44135	1
Dr. B. Brummer EIC Incorporated 55 Chapel Street Newton, Massachusetts 02158	1
Library P. R. Mallory and Company, Inc. Northwest Industrial Park Burlington, Massachusetts 01803	1
Dr. P. J. Hendra Department of Chemistry University of Southampton Southampton S00 5NH United Kingdom	
Dr. Sam Perone Chemistry & Materials Science Department Laurence Livermore National Lab. Livermore, California 94550	
Dr. Royce W. Murray Department of Chemistry University of North Carolina Chapel Hill, North Carolina 27514	
Naval Ocean Systems Center Attn: Technical Library San Diego, California 92152	
Dr. C. E. Mueller The Electrochemistry Branch Materials Division, Research and Technology Department Naval Surface Weapons Center White Oak Laboratory Silver Spring, Maryland 20910	
Dr. G. Goodman Johnson Controls 5757 North Green Bay Avenue Milwaukee, Wisconsin 53201	
Dr. J. Boechler Electrochimica Corporation Attn: Technical Library 2485 Charleston Road Mountain View, California 94040	
Dr. P. P. Schmidt Department of Chemistry Oakland University Rochester, Michigan 48063	

TECHNICAL REPORT DISTRIBUTION LIST, GEN

	No. Copies
Office of Naval Research Attn: Code 413 800 North Quincy Street Arlington, Virginia 22217	2
ONR Pasadena Detachment Attn: Dr. R. J. Marcus 1030 East Green Street Pasadena, California 91106	1
Commander, Naval Air Systems Command Attn: Code 310C (H. Rosenwasser) Department of the Navy Washington, D.C. 20360	1
Defense Technical Information Center Building 5, Cameron Station Alexandria, Virginia 22314	12
Dr. Fred Saalfeld Chemistry Division, Code 6100 Naval Research Laboratory Washington, D.C. 20375	1
U.S. Army Research Office Attn: CRD-AA-IP P. O. Box 12211 Research Triangle Park, N.C. 27709	1
Mr. Vincent Schaper DTNSRDC Code 2803 Annapolis, Maryland 21402	1
Naval Ocean Systems Center Attn: Dr. S. Yamamoto Marine Sciences Division San Diego, California 91232	1
Naval Ocean Systems Center Attn: Mr. Joe McCartney San Diego, California 92152	
Naval Weapons Center Attn: Dr. A. B. Amster, Chemistry Division China Lake, California 93555	
Naval Civil Engineering Laboratory Attn: Dr. R. W. Drisko Port Hueneme, California 93401	
Dean William Tolles Naval Postgraduate School Monterey, California 93940	
Scientific Advisor Commandant of the Marine Corps (Code RD-1) Washington, D.C. 20380	
Naval Ship Research and Development Center Attn: Dr. G. Bosmajian, Applied Chemistry Division Annapolis, Maryland 21401	
Mr. John Boyle Materials Branch Naval Ship Engineering Center Philadelphia, Pennsylvania 19112	
Mr. A. M. Anzalone Administrative Librarian PLASTEC/ARRADCOM Bldg 3401 Dover, New Jersey 07801	

VI. Personnel

A. Faculty

Y.W. Chung - Principal Investigator - Associate Professor
P.C. Stair - Principal Investigator - Associate Professor
G.C. Schatz - Principal Investigator - Professor
R.P. Van Duyne - Principal Investigator - Professor
E. Weitz - Principal Investigator - Professor

B. Graduate Students

D.R. Burgess
M. Moser
D. Decrease
J. Livermore
G. Daghita
M. Barr
N. Schultz
A. Ouderkirk

C. Postdoctorals

R. Viswanathan
I. Hussla
U. Laor
P.K.K. Pandey
W.A. Kraus
A. Stacy
J. Haushalter
C. Gallucci
M. Matyjasczyzk
M. Johnston

D. Other

R.D. Bates, Jr. - Visiting Scholar - Associate Professor - Georgetown University

18. U. Laor and G.C. Schatz, Chem. Phys. Lett., 82, 566-570 (1981).

19. G.C. Schatz in "Surface Enhanced Raman Scattering", R.K. Chang and T.E. Furtak, Eds., Plenum, New York, 1982, pages 35-50.

20. U. Laor and G.C. Schatz, J. Chem. Phys., 76, 2888-2899 (1982).

21. P.K.K. Pandey and G.C. Schatz, Chem. Phys. Lett., 88, 193-197 (1982).

22. P.K.K. Pandey and G.C. Schatz, Chem. Phys. Lett., 91, 286-290 (1982).

23. P.K.K. Pandey and G.C. Schatz, J. Electron Spectroscopy and Related Phenomena, 29, 351-355 (1983).

V. Publications Acknowledging Support of N00014-79-C-0794

1. R. Viswanathan, D.R. Burgess, Jr., P.C. Stair and E. Weitz, J. Vac. Sci. Technol. 20, 605 (1982).

2. R. Viswanathan, D.R. Burgess, Jr., P.C. Stair and E. Weitz, J. Electron. Tech. Rel. Phenom. 29, 111 (1983).

3. D.R. Burgess, Jr., R. Viswanathan, I. Hussla, P.C. Stair and E. Weitz, J. Chem. Phys. 79, 5200 (1983).

4. D.R. Burgess, Jr., I. Hussla, P.C. Stair, R. Viswanathan and E. Weitz, Rev. Sci. Instrum. 55, 1771 (1984).

5. D.R. Burgess, Jr., Ph.D. Thesis, Northwestern University, 1/85.

6. M.D. Moser and E. Weitz, Chem. Phys. Letters 82, 285 (1981).

7. M.D. Moser, E. Weitz and G.C. Schatz, J. Chem. Phys. 78, 757 (1983).

8. I. Hussla and R. Viswanathan, Surf. Sci. 145, 2488 (1984).

9. I. Hussla and R. Viswanathan, Proceedings Int. Conf. on Laser Processing and Diagnostics, Springer Series in Chemical Physics, in press.

10. C.S. Allen, G.C. Schatz and R.P. Van Duyne, Surf. Sci., 101, 425-438 (1980).

11. C.S. Allen, G.C. Schatz and R.P. Van Duyne, Chem. Phys. Letters, 75, 201-205, (1980).

12. K.D. Parks and R.P. Van Duyne, Chem. Phys. Letters, 76, 196-200 (1980).

13. S.G. Schultz, M. Janik-Czachor and R.P. Van Duyne, Surf. Sci., 104, 419-434 (1981).

14. C.S. Allen and R.P. Van Duyne, J. Am. Chem. Soc., 103, 7497-7501 (1981).

15. S.G. Schultz, T.M. Cotton and R.P. Van Duyne, J. Am. Chem. Soc., 104, 6528-6532 (1982).

16. M. Janik-Czachor and R.P. Van Duyne, J. Electrochem. Soc., 130, 2320-2323 (1983).

17. G. C. Schatz and R. P. Van Duyne, Surf. Sci., 101, 425-438 (1980).

37. U. Laor and G.C. Schatz, J. Chem. Phys., 76, 2888-2899 (1982).

38. P.K.K. Pandey and G.C. Schatz, Chem. Phys. Lett., 88, 193-197 (1982).

39. P.K.K. Pandey and G.C. Schatz, Chem. Phys. Lett., 91, 286-290 (1982).

40. P.K.K. Pandey and G.C. Schatz, J. Electron Spectroscopy and Related Phenomena, 29, 351-355 (1983).

18. K.T. Carron, T.M. Cotton, J.P. Haushalter, and R.P. Van Duyne, J. Am. Chem. Soc., (submitted).

19. A.B. Apkarian and R.P. Van Duyne, Surf. Sci., (submitted).

20. A.B. Apkarian and R.P. Van Duyne, Surf. Sci., (in preparation).

21. M. Barr, A. Stacey, P. Stair and R.P. Van Duyne, Surf. Sci., (in preparation).

22. M. Barr, A. Stacey, P. Stair and R.P. Van Duyne, Surf. Sci., (in preparation).

23. A. Stacey and R.P. Van Duyne, J. Chem. Phys., (in preparation).

24. M.V. Johnston and R.P. Van Duyne, Chem. Phys. Lett. (in preparation).

25. M.V. Johnston, J. Roper and R.P. Van Duyne, J. Phys. Chem. (in preparation).

26. M.V. Johnston, J. Roper and R.P. Van Duyne, Appl. Phys. Letters (in preparation).

27. B.H. Loo, J. Chem. Phys. 75, 5955 (1981).

28. R.K. Chang and T.E. Furtak, Eds., "Surface Enhanced Raman Scattering," Plenum Press, New York, 1982.

29. I. Pockrand, Chem. Phys. Lett., 85, 37 (1982).

30 D.L. Jeanmaire and R.P. Van Duyne, J. Electroanal. Chem. 84, 1 (1977).

31. R.P. Van Duyne, J. Phys. (Paris) 38, C5-239 (1977).

32. R.P. Van Duyne, in "Chemical and Biochemical Applications of Lasers," Vol. 4, C.B. Moore, Ed., Academic Press, New York, 1979, pgs. 101-185.

33. I.K. Schuller and C.M. Falco, in "VLSI Electronics: Microstructure Sciences" Vol. 4, N.G. Einspruch, Ed., p. 183-205, Academic Press, N.Y., 1982.

34. G. C. Schatz and R. P. Van Duyne, Surf. Sci., 101, 425-438 (1980).

35. U. Laor and G.C. Schatz, Chem. Phys. Lett., 82, 566-570 (1981).

36. G.C. Schatz in "Surface Enhanced Raman Scattering", R.K. Chang and T.E. Furtak, Eds., Plenum, New York, 1982, pages 35-50.

IV. REFERENCES

1. R. Viswanathan, D.R. Burgess, Jr., P.C. Stair and E. Weitz, J. Vac. Sci. Technol. 20, 605 (1982).

2. R. Viswanathan, D.R. Burgess, Jr., P.C. Stair and E. Weitz, J. Electron. Spec. Rel. Phenom. 29, 111 (1983).

3. D.R. Burgess, Jr., R. Viswanathan, I. Hussla, P.C. Stair and E. Weitz, J. Chem. Phys. 79, 5200 (1983).

4. D.R. Burgess, Jr., I. Hussla, P.C. Stair, R. Viswanathan and E. Weitz, Rev. Sci. Instrum. 55, 1771 (1984).

5. J.C. Tracy, J. Chem. Phys. 56, 2748 (1972).

6. J.P. Cowin, D.J. Auerbach, C. Becker and L. Wharton, Surf. Sci. 78, 545 (1978).

7. J.C. Tully, Surf. Sci. 111, 461 (1981).

8. C.S. Allen, G.C. Schatz and R.P. Van Duyne, Surf. Sci., 101, 425-438 (1980).

9. C.S. Allen, G.C. Schatz and R.P. Van Duyne, Chem. Phys. Letters, 75, 201-205, (1980).

10. K.D. Parks and R.P. Van Duyne, Chem. Phys. Letters, 76, 196-200 (1980).

11. S.G. Schultz, M. Janik-Czachor and R.P. Van Duyne, Surf. Sci., 104, 419-434 (1981).

12. C.S. Allen and R.P. Van Duyne, J. Am. Chem. Soc., 103, 7497-7501 (1981).

13. S.G. Schultz, T.M. Cotton and R.P. Van Duyne, J. Am. Chem. Soc., 104, 6528-6532 (1982).

14. M. Janik-Czachor and R.P. Van Duyne, J. Electrochem. Soc., 130, 2320-2323 (1983).

15. C.S. Allen and R.P. Van Duyne, J. Phys. Chem., submitted.

16. C.S. Allen and R.P. Van Duyne, Surf. Sci., (in preparation).

17. J.M. Lakovits and R.P. Van Duyne, J. Electroanal. Chem., (submitted).

other possible enhancement processes is expected to vary with the nature of the adsorbate and metal, we are not yet in a position to make the generalization of these conclusions to other systems. Additional calculations are now underway to provide this important generalization.

Note that these results refer to Li clusters for which the excited state widths have been equated to those for bulk Li metal. This removes the surface scattering component from the orbital widths, and thus makes our enhancements directly comparable to those for larger Li clusters such as have been studied by Moskovits and DiLella. Since the experiments refer to N_2 on Li_n rather than H_2 on Li_n, a direct comparison of theory and experiment is not possible yet. It does appear however that the experimentally measured enhancement is close to what we have calculated.

The dependence of the enhancement on the distance from the surface has provided interesting clues (which are not yet fully analyzed) as to the nature of the enhancement mechanism. For distances greater than the equilibrium adsorption distance, the enhancement decreases with increasing distance according to what one would expect from the electromagnetic mechanism. At shorter distances, however, the enhancement shows a more rapid rise which appears to be due to a short ranged mechanism. Detailed analysis of the polarizability expression indicates that the dominant short range mechanism is due to modulation of the metal orbital energies by the molecular vibrational displacements. This is somewhat like the previously proposed Raman reflection mechanism of SERS enhancement whereby modulation of the metal dielectric constant by adsorbed molecule vibrational motions causes a Raman component in reflectance from the metal. This is also related to a number of charge transfer mechanisms which are being explored since the metal orbital energy modulation is due (in part) to the transfer of electron density to and from molecular and metal atomic orbitals. Since the interplay between the electromagnetic mechanism, energy modulation and

Ab Initio Calculations of SERS Intensities:

In view of the above described results concerning the failure of the electromagnetic mechanism to describe all of the enhancement observed in SERS, we have initiated an ab initio study of molecule-metal surface spectroscopy to study short range enhancement mechanisms. The calculations refer to molecules adsorbed onto small metal clusters. Hartree-Fock (HF) methods are used to determine static properties of the clusters such as equilibrium geometries, frequencies and molecular orbitals, and then time dependent Hartree-Fock (TDHF) methods are used to calculate the frequency dependent polarizability derivatives whose squares are proportional to the Raman cross sections. By comparing such information for the molecule on and off the cluster, surface enhancements are determined.

While the computational methodology associated with the HF calculation is standard, that for the TDHF evaluation is not. In particular, the evaluation of polarizability derivatives at frequencies which are close to resonance in the metal requires a non-iterative evaluation of the first order density matrix. Special techniques have been developed for doing this, including a basis set selection procedure which helps to identify metal cluster states which are important in determining the SERS intensities.

The results of these calculations to date have been for H_2 adsorbed onto lithium clusters of the type Li_n ($n = 2, 4, 6$). These calculations indicate that when H_2 is at its equilibrium adsorption geometry, the Raman intensities for the H_2 stretch are enhanced by about 10^4. The precise value of the enhancement depends on the adsorption site, adsorbate orientation and cluster size.

than 10^4, and more likely about 10^3. These maximums are smaller than what can be obtained for single spheroids, but are spread out over a broader region of the spectrum. Third, hemispheroids do not have to be highly prolate in order to have collective plasmon resonances at frequencies significantly lower than the isolated hemispheroid plasmon frequency. Indeed, groups of closely packed hemispheroids can show multiple resonances which for a metal like silver can be spread throughout the visible. Fourth, the change in enhancement in going from a strong SERS metal like Ag to one which shows no SERS activity like Pt is less than 10^2. This change is at least one order of magnitude smaller than is needed to explain experimental observations. This, and the $< 10^6$ calculated enhancement maximums suggest that the electromagnetic mechanism is not the only enhancement mechanism operative in SERS.

Local Field Enhancements on Randomly Roughened Surfaces:

Although there have been several attempts to evaluate SERS enhancements arising from the electromagnetic mechanism (i.e., enhanced local fields due to surface plasmon excitation), only our work has considered randomly roughened surfaces such as are present in electrochemically anodized and some vapor deposited metal surfaces. Given the wealth of SERS data on such surfaces, including data obtained with surfaces having different bump distributions and sizes, the development of theoretical methods for estimating local field enhancements on such surfaces has provided an important link in evaluating the electromagnetic mechanism.

Most of our work in this area has concentrated on a model of the electrodynamics for random distributions of metal hemispheroids on flat surfaces. The interactions between different hemispheroids are approximated by the leading (dipole) term, but the field close to each hemispheroid is treated with an accurate solution of LaPlace's equation. This compromise between accuracy and simplicity enables us to treat both random and nonrandom distributions of hemispheroids of arbitrary heights and widths quite easily, and thereby to assess the metal and frequency dependence of the enhancement for a wide variety of metals.

Our results to date have lead to several significant conclusions. First, the magnitude of the enhancement and its frequency dependence is not strongly dependent on the exact nature of the size and shape distributions of the hemispheroids as long as they are closely packed on the surface. Second, the maximum enhancements calculated from this mechanism for Ag, Cu and Au are less

TECHNICAL REPORT DISTRIBUTION LIST, 359

	No. Copies
Dr. Donald W. Ernst Naval Surface Weapons Center Code R-33 White Oak Laboratory Silver Spring, Maryland 20910	1
Dr. R. Nowak Naval Research Laboratory Code 6130 Washington, D.C. 20375	1
Dr. John F. Houlihan Shenango Valley Campus Pennsylvania State University Sharon, Pennsylvania 16146	1
Dr. D. F. Shriver Department of Chemistry Northwestern University Evanston, Illinois 60201	1
Dr. D. H. Whitmore Department of Materials Science Northwestern University Evanston, Illinois 60201	1
Dr. Alan Bewick Department of Chemistry The University Southampton, SO9 5NH England	
Dr. A. Himy NAVSEA-5433 NC #4 2541 Jefferson Davis Highway Arlington, Virginia 20362	
Dr. John Kincaid Kaman Sciences Corporation 1911 Jefferson Davis Hwy., Suite 1200 Arlington, Virginia 22202	
Mr. James R. Moden Naval Underwater Systems Center Code 3632 Newport, Rhode Island 02840	
Dr. Bernard Spielvogel U. S. Army Research Office P. O. Box 12211 Research Triangle Park, NC 27709	
Dr. Denton Elliott Air Force Office of Scientific Research Bolling AFB Washington, D.C. 20332	
Dr. David Aikens Chemistry Department Rensselaer Polytechnic Institute Troy, New York 12181	
Dr. A. P. B. Lever Chemistry Department York University Downsview, Ontario M3J1P3 Canada	
Dr. Stanislaw Szpak Naval Ocean Systems Center Code 6343 San Diego, California 95152	
Dr. Gregory Farrington Department of Materials Science and Engineering University of Pennsylvania Philadelphia, Pennsylvania 19104	
Dr. Bruce Dunn Department of Engineering & Applied Science University of California Los Angeles, California 90024	

TECHNICAL REPORT DISTRIBUTION LIST, 359

	No. Copies
M. L. Robertson Manager, Electrochemical and Power Sonices Division Naval Weapons Support Center Crane, Indiana 47522	1
Dr. Elton Cairns Energy & Environment Division Lawrence Berkeley Laboratory University of California Berkeley, California 94720	1
Dr. Micha Tomkiewicz Department of Physics Brooklyn College Brooklyn, New York 11210	1
Dr. Lesser Blum Department of Physics University of Puerto Rico Rio Piedras, Puerto Rico 00931	1
Dr. Joseph Gordon, II IBM Corporation K33/281 5600 Cottle Road San Jose, California 95193	1
Dr. Robert Somoano Jet Propulsion Laboratory California Institute of Technology Pasadena, California 91103	1
Dr. Johann A. Joebstl USA Mobility Equipment R&D Command DRDME-EC Fort Belvior, Virginia 22060	1
Dr. Judith H. Ambrus NASA Headquarters M.S. RTS-6 Washington, D.C. 20546	1
Dr. Albert R. Landgrebe U.S. Department of Energy M.S. 6B025 Forrestal Building Washington, D.C. 20595	1
Dr. T. Marks Department of Chemistry Northwestern University Evanston, Illinois 60201	
Dr. D. Cipris Allied Corporation P. O. Box 3000R Morristown, New Jersey 07960	
Dr. M. Philpot IBM Corporation 5600 Cottle Road San Jose, California 95193	
Dr. Donald Sandstrom Washington State University Department of Physics Pullman, Washington 99164	
Dr. Carl Kannewurf Northwestern University Department of Electrical Engineering and Computer Science Evanston, Illinois 60201	
Dr. Edward Fletcher University of Minnesota Department of Mechanical Engineering Minneapolis, Minnesota 55455	
Dr. John Fontanella U.S. Naval Academy Department of Physics Annapolis, Maryland 21402	
Dr. Martha Greenblatt Rutgers University Department of Chemistry New Brunswick, New Jersey 08903	
Dr. John Wassib Kings Mountain Specialties P. O. Box 1173 Kings Mountain, North Carolina 28086	

TECHNICAL REPORT DISTRIBUTION LIST, 359

	No. Copies
Dr. J. J. Brophy University of Utah Department of Physics Salt Lake City, Utah 84112	1
Dr. Walter Roth Department of Physics State University of New York Albany, New York 12222	1
Dr. Thomas Davis National Bureau of Standards Polymer Science and Standards Division Washington, D.C. 20234	1
Dr. Charles Martin Department of Chemistry Texas A&M University	1
Dr. Anthony Sammells Institute of Gas Technology 3424 South State Street Chicago, Illinois 60616	1
Dr. H. Tachikawa Department of Chemistry Jackson State University Jackson, Mississippi 39217	1
Dr. W. M. Risen Department of Chemistry Brown University Providence, Rhode Island	1

END

FILMED

5-85

DTIC